Adaptive Frequency Resolution for Downlink Beamforming in 5G NR

JOHANNA BENGTSSON
MASTER´S THESIS
DEPARTMENT OF ELECTRICAL AND INFORMATION TECHNOLOGY
FACULTY OF ENGINEERING | LTH | LUND UNIVERSITY

Adaptive Frequency Resolution for Downlink Beamforming in 5G NR

Johanna Bengtsson
geo15jbe@student.lu.se

Department of Electrical and Information Technology
Lund University

Supervisor: Harish Venkatraman Bhat, Ericsson AB
Fredrik Tufvesson, LTH

Examiner: Fredrik Rusek

June 20, 2021

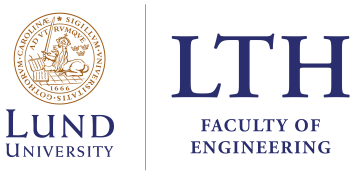

Printed in Sweden
Tryckeriet i E-huset, Lund

Abstract

As the demand for higher data rates and lower latencies increase, together with the use of higher frequency bands, MIMO and beamforming have become an essential part of the 5G NR technology. Calculating the beamforming weights is a costly process, and reducing the frequency resolution of the weight calculations would save a significant amount of computational power. Which resolution is suitable to use depends on the channel's frequency selectivity, which can be measured by for instance the RMS Delay Spread.

This thesis analyzes two algorithms for adaptive resolution of the beamforming weights. The main focus of the work lies on the first algorithm, one that analyzes the channel estimation from the uplink and selects a suitable resolution for the downlink beamforming weight calculations. First, suitable thresholds for the resolutions and decision parameters were estimated through simulations, after which the performance of the algorithm could be evaluated. The impact of number of antennas and number of UEs was also explored. The second algorithm is simpler in nature, where the resolution is maximized while maintaining a lower limit of errors. The development and evaluation of the algorithms was performed through Matlab simulations.

Populärvetenskaplig Sammanfattning

Sedan den första generationen av mobila nätverk lanserades i början av 80-talet har en ny generation utvecklats ungefär vart tionde år. Med ett alltmer digitaliserat samhälle har användningen av de mobila nätverken ökat drastiskt. Ökningen ställer nya krav på nätverkens kapacitet där den senaste generationen, 5G NR, är utvecklad för att tillgodose dagens och kommande års behov. Dessa behov innefattar bland annat större mängder data och låga fördröjningar. En teknik som används i 5G NR för att både öka prestandan och öppna för nya funktioner är lobformning. Vid lobformning samverkar flera antenner för att rikta sändande och mottagande av signalen, vilket leder till att signalstyrkan hos användaren ökar.

För att utföra lobformning från en basstation till en användare används kanalestimat för att vikta den data som ska sändas. För att uppnå maximal prestanda skulle vikterna beräknas på symbolnivå, alltså att den korrekta viktningen för varje symbol som sänds hade beräknats. Beräkningarna är dock tidskrävande, och med ett stort antal antenner växer också deras komplexitet. Detta gör att det inte är genomförbart att beräkna vikterna med så hög upplösning i ett realtidssystem med begränsade resurser. En möjlig lösning är att sätta en statisk lägre upplösning för att minska komplexiteten, vilket dock kan leda till dålig prestanda eller onödigt hög upplösning. Detta då vilken upplösning som passar bäst beror på den trådlösa kanalens egenskaper.

I det här arbetet har en algoritm utvecklats för att anpassa upplösningen efter radiokanalens egenskaper. Beslutet om vilken upplösning som är bäst lämpad fattas genom analys av kanalen, där olika volatilitet i frekvenssvaret ger olika upplösningar. Tre olika mått på kanalen utvärderades som grund för estimeringen, och algoritmen utvecklades och testades genom Matlab-simuleringar.

Resultaten visar att det är möjligt att genom analys av den trådlösa kanalen uppskatta en passande upplösning för lobformning, där upplösningen kunde sänkas samtidigt som prestandan hölls vid en likvärdig nivå.

Acknowledgements

I would like to express my gratitude towards Harish Venkatraman Bhat and Mladen Toncev for giving me the opportunity to carry out this master thesis at Ericsson. I would like to direct a special thanks to Harish for being a great supervisor throughout the thesis, and to Juan Guirado Lopez-Puigcerver for all the help getting started. I also want to thank Fredrik Tufvesson, my supervisor at LTH, for very valuable input on the thesis work and a firm belief in my abilities.

Finally, I want to thank all of my friends that are finishing this education alongside me. Studying has been much more pleasurable in your company than it could ever be alone.

Table of Contents

List of Figures

List of Tables

List Of Abbreviations

3GPP	The 3rd Generation Partnership Project
ABF	Average Bandwidth of Fades
BER	Bit Error Rate
BPSK	Binary Phase Shift Keying
BS	Base Station
cdf	Cumulative Distribution Function
CRC	Cyclic Redundancy Check
CSI	Channel State Information
CSI-RS	Channel State Information Reference Signal
DFT	Discrete Fourier Transform
DL-SCH	Downlink Shared Channel
DMRS	Demodulation Reference Signal
DSP	Digital Signal Processor
FDD	Frequency Division Duplex
gNB	g-node B
GSM	Global System for Mobile Communications
GUI	Graphical User Interface
IFFT	Inverse Fast Fourier Transform
IoT	Internet of Things
ISI	Inter Symbol Interference
LCR	Level Crossing Rate
LDPC	Low Density Parity Check
LOS	Line-of-Sight
LTE	Long Term Evolution
MCS	Modulation and Coding Scheme
MIMO	Multiple-Input Multiple-Output
MMSE	Minimum Mean Square Error
MRT	Maximum Ratio Transmission
MU-MIMO	Multi-User MIMO
NLOS	Non Line-of-Sight
NR	New Radio
OFDM	Orthogonal Frequency Division Multiplexing
OFDMA	Orthogonal Frequency Division Multiplexing Access
PBCH	Physical Broadcast Channel
PDCCH	Physical Downlink Control Channel
PDP	Power Delay Profile
PDSCH	Physical Downlink Shared Channel
PRACH	Physical Random-Access Channel
PRB	Physical Resource Block
PUCCH	Physical Uplink Control Channel
PUSCH	Physical Uplink Shared Channel
QAM	Quadrature Amplitude Modulation
QPSK	Quadrature Phase Shift Keying
RB	Resource Block
RMS	Root Mean Square

Rx	Receiver
RZF	Regularized Zero Forcing
SINR	Signal to Interference plus Noise Ratio
SNR	Signal to Noise Ratio
SRS	Sounding Reference Signal
SU-MIMO	Single-User MIMO
TDD	Time Division Duplex
Tx	Transmitter
UE	User Equipment
UL-SCH	Uplink Shared Channel
ZF	Zero Forcing

Chapter 1

Introduction

This section gives background information and motivates the need for this thesis work. It also covers the main points included in the thesis, and the outline of this report.

1.1 Background and Motivation

Ever since the first generation cellular networks, there has been a new generation developed every 10 years. With each generation follows a new infrastructure, new standards and new use cases to satisfy. In 5G NR, the latest generation of cellular networks, the use of multiple antenna systems has become crucial due to the higher frequency regions of operation. One possibility of using multiple antennas is beamforming, where the signal is directed towards a user instead of being transmitted omnidirectionally. This increases the performance of the system, however also demanding more resources. As the number of antennas grow, the complexity is further increased and more computational resources are required to perform the beamforming.

1.2 Thesis Purpose and Aims

The purpose of the thesis is to explore the possibilities to adapt the frequency resolution of the beamforming weights to the wireless channel. This is attempted by two algorithms proposed in the thesis, where the resolution is adapted in two different ways.

- *Adaptive Frequency Resolution Algorithm* Minimize the resolution while

aiming to maintain the same BER for the link. This algorithm is referred to as *Adaptive Frequency Resolution Algorithm* in the report.

- *Adaptive Frequency Resolution - BER Limit Algorithm* Minimize the resolution while keeping the BER under a pre-defined threshold. This algorithm is referred to as *BER Limit Algorithm* in the report.

The main focus of the thesis lies on the first algorithm, where the BER is maintained while the resolution is lowered. To achieve this, the frequency response of the channel is analyzed and used as a basis for the resolution decision in the algorithm. Different measures for the frequency selectivity of the channel are evaluated. The second algorithm does not require analysis of the frequency response, but only uses the BER to lower the resolution as much as possible. The performance of both algorithms is evaluated based on the increase of BER and decrease in resolution. Matlab simulations of the NR transmission chain are used for development and evaluation of the algorithm.

1.3 Thesis Outline

The thesis begins with presenting theory relevant for understanding the thesis work. An overview of 5G NR, presenting the evolution of NR and the main use cases, is followed by a description of the most relevant parts of the 5G NR physical layer. The thesis continues to present wireless channels and some properties of the channel frequency response, and the theoretical background ends with relevant information on multiple antenna systems and beamforming.

Then follows a description of the proposed algorithms, after which the methodology is described. This section includes information on the simulation model and simulation scenarios designed for the algorithm development and evaluation. The succeeding section presents the results, and the final chapter holds conclusions and future scope of the thesis work.

Chapter 2

NR Overview

This section presents the evolution of 5G NR, its precursors and important aspects of the technology. A review of the use cases to be covered by 5G NR is also given.

2.1 Evolution of 5G NR

Today's society is becoming increasingly dependent on mobile communications. The technologies have provided a solid ground for both economic growth and improvements of social circumstances globally, and will continue to be a crucial asset to society for the forseeable future.

The development of mobile communications began with support of analog phone calls in the 1980s. The second generation, released in 1991, was the first one to utilize the globally standardized digital transmission technology GSM [7]. The third generation increased the data rates significantly, leading up to the release of 4G LTE. LTE provided even higher data rates and with smartphones released with close proximity in time, the use of the mobile network increased dramatically.

While LTE became extremely successful and still provides reliable service to billions of users, the next generation radio access technology has been standardized and is under development as 5G NR. The development is motivated by several new use cases where LTE is working but is not an optimal technology. One main difference between 5G NR and LTE is the supported frequency bands. The spectrum of the first release of 5G NR stretches up to 52.6 GHz, while LTE only operates up to around 3.5 GHz [6]. Operation in a wider frequency range increases the spectral resources significantly, which in turn allows higher speeds and larger volumes of data over the network.

To efficiently use the spectral resources, multi-antenna technologies are used.

Multiple antennas are already commonly used in LTE to increase diversity, directivity and allow for spatial multiplexing. The motivations remain for using multiple antenna systems in NR, with the critical addition that the higher frequencies result in higher path losses and thus reduced range when keeping the transmission power within legal levels [7]. Larger bandwidth also increase the thermal noise levels, and both factors make the use of multiple antennas critical.

The evolution of 5G has been carried out in parallel with continous advancements of LTE. Seeing LTE as a foundation of the 5G solutions, 3GPP has released the specifications for 5G NR in two steps. The first release in 2018, release 15, focused on utilizing higher frequency bands and larger bandwidths while coexisting and being aided by existing LTE infrastructure. This is referred to as non-standalone 5G. The standalone version was released only 6 months later, and is intended to operate independently from LTE while still co-existing with the technology.

The second release, release 16, includes specifications on multiple antenna systems and beamforming, spectrum sharing between LTE and NR, and energy efficiency. It also covers UE positioning and the use cases of industrial Internet of Things (IoT) and vehicular communication systems [21].

2.2 Use Cases

There are a large number of use cases that motivates the standardization and development of NR. The ones listed below can be seen as very general use cases and form a base for more specific use cases.

- *High data rates and larger volumes of data.* This continues the evolution that has been going on since the first generation mobile networks, and was the main use case for LTE to cover. As the utilization of mobile networks increases and the world becomes more digitized, the need for fast transmission of large amounts of data continues to grow.
- *Support for a large number of connected devices.* With the rise of Internet of Things (IoT), the amount of connected devices is predicted to escalate. While the number of devices will be large, the amount of data sent by an IoT device is usually small. The LTE technology is not optimized for such machine-type communications [20].
- *Low power consumption.* The aim for most IoT devices is to run for a long period of time on a battery, which requires extremely energy efficient solutions. A network optimized for low power devices will aid the process of developing truly energy efficient IoT solutions.
- *Low latency.* The time it takes for the data to go from source to destination is called latency. With the research and development within areas such as

vehicular communication systems and industrial automation, low latency and reliable connections becomes critical [7].

The term 5G is in in many cases not seen as its own radio access technology, but as the technology that satisfies the use cases defined to be covered [7]. The radio technologies are in many cases identical to those of LTE, but assembled to a significantly more dynamic system. Therefore, identifying the desired use cases was an important step prior to the 3GPP standardization.

Chapter 3

Physical Layer of 5G NR

This section presents the physical layer aspects of NR most relevant for understanding the thesis work. As the Matlab simulation model used for the project was originally implemented in accordance with 3GPP specifications of LTE and later adjusted to NR, understanding of uplink and downlink procedures is crucial.

3.1 Physical Resources in NR

There are 5 different numerologies in NR. Each numerology corresponds to a cyclic prefix length, which will be further explained in section 3.4, and subcarrier spacing configuration that can be used during transmission. The different properties of the numerologies are presented in Table 3.1 where μ is numerology index and $\Delta f = 2^{\mu} \times 15$ [kHz] the subcarrier spacing.

μ	Δf [kHz]	Cyclic Prefix Length
0	15	Normal
1	30	Normal
2	60	Normal, Extended
3	120	Normal
4	240	Normal

Table 3.1: Table of numerologies in NR [2]

All information transmitted in NR is divided into frames. Each frame spans 10 ms in the time domain and is in turn divided into 10 subframes of length 1 ms each. The frames are further divided into two half-frames each consisting of

five subframes [2]. The bandwidth of the frame depends on the channel bandwidth used for the specific carrier. The number of slots per subframe depends on the numerology and the frame structure for numerology $\mu = 2$ is illustrated in Figure 3.1.

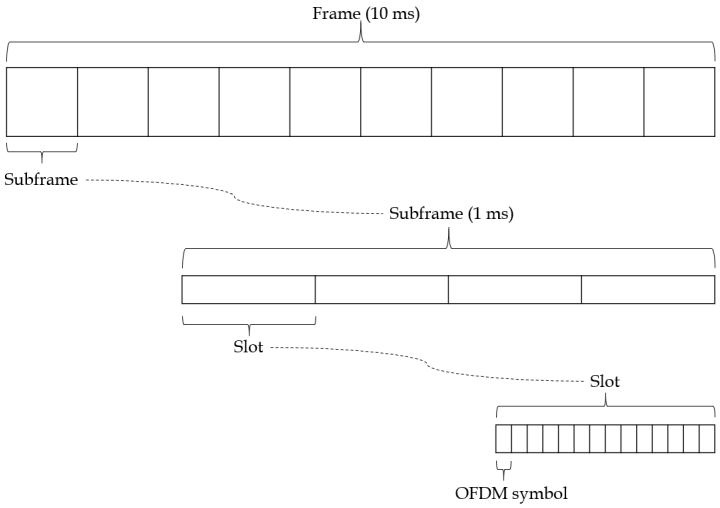

Figure 3.1: The frame structure in NR for numerology $\mu = 2$, normal CP length.

A resource grid can be defined for each numerology. The grid for one slot spaces all subcarriers in frequency and the number of OFDM symbols per slot in time. The length in time is 14 OFDM symbols for normal cyclic prefix length. The resources are divided into physical resource blocks (PRB) of 12 subcarriers in the frequency domain and one slot in the time domain each [2]. The smallest unit defined is the resource element (RE), which consists of one subcarrier and one OFDM symbol. Use of multiple antennas adds the possibility of spatial multiplexing, which gives one resource grid per antenna port. Antenna ports are ports where the channel between one UE antenna and the antenna port can be assumed to be the same for two signals transmitted from the same port. If a signal is transmitted from a different antenna port, the channel must be different. An illustration of the grid structure can be found in Figure 3.2. The total bandwidth of a PRB depends on the subcarrier spacing, which in turn depends on the numerology μ.

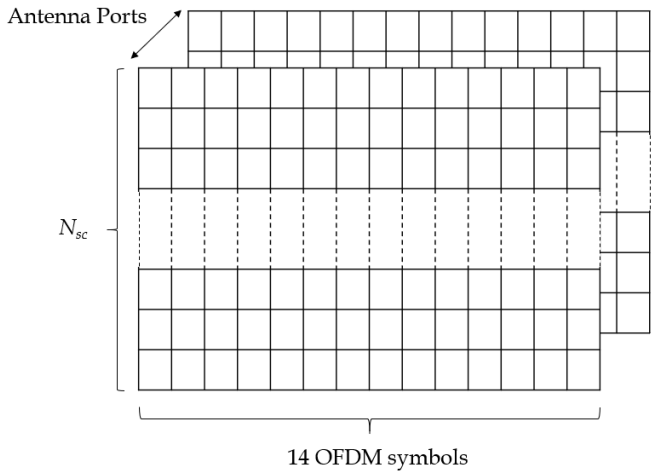

Figure 3.2: Resource grid structure in NR for normal cyclic prefix length where N_{sc} is number of subcarriers.

3.2 Physical Channels in NR

There are three different physical channels for uplink and downlink respectively in NR. Which channel a signal is transmitted over depends on the type of information that the signal carries. These physical channels are later mapped to different higher layer channels.

3.2.1 Uplink Channels

For uplink the channels PUSCH, PRACH and PUCCH are defined [7].

- *PUSCH Physical Uplink Shared Channel* is the channel that transports user data and control data for the higher layers.
- *PUCCH, Physical Uplink Control Channel* carries control signals for channel estimation and is also used for acknowledgements of received data.
- *PRACH, Physical Random-Access Channel* transmits a preamble used for channel access

3.2.2 Downlink Channels

For downlink, the corresponding channels are PDSCH, PDCCH and PBCH [7].

- *PDSCH, Physical Downlink Shared Channel* is the downlink counterpart to PUSCH and carries user data and higher layer control data.
- *PDCCH, Physical Downlink Control Channel* corresponds to the PUCCH channel and carries physical layer control signals.
- *PBCH, Physical Broadcast Channel* broadcasts information about how to access the network.

3.3 Modulation and Coding Scheme, MCS

NR uses a lookup-table for determining the appropriate Modulation and Coding Scheme (MCS). Each MCS option consists of a modulation order and code rate for the channel coding.

The modulation order defines the number of bits per symbol as *Modulation Order* $= 2^n$ where n is the number of bits transmitted per symbol. The MCS tables for NR include the modulation QPSK, 16-QAM, 64-QAM and 256-QAM, or the modulation *orders* n = 2, 4, 6, 8 [3]. Channel coding is a technique where redundancy is added to the information bits. The redundant bits can be used to detect and correct errors at the receiver, and the number of correctable errors depends on the type of coding and the code rate. The code rate is the ratio between the information bits and the total number of transmitted bits

$$R = \frac{k}{n}, \tag{3.1}$$

where k is the number of information bits and $n - k$ is the number of redundant bits. In NR, LDPC codes are used for both the uplink and downlink shared channels. LDPC code stands for Low Density Parity-Check code and is a type of linear error correcting block code [14]. The code consists of several low-complexity component codes which allows large blocks of information to be encoded without an unmanagable decoding procedure. Larger blocks yield stronger codes, which makes LDPC codes a very effective coding scheme allowing the throughput to approach the Shannon Limit. The Shannon Limit is a theoretical limit for error-free throughput over a channel of certain bandwidth and noise, and is often referred to as channel capacity. It is given by

$$R = B\,log_2(1 + SNR) \;\; [bps], \tag{3.2}$$

where R is the information data rate, B is the bandwidth and SNR the signal to noise ratio [14].

Modulation order and code rate together define the spectral efficiency of the channel. The choice of MCS is thus a choice of how much spectral resources should be utilized for information transmission. The decision is based on the estimated SNR of the channel. A higher quality of the channel allows for a higher spectral efficiency.

3.4 OFDM

Orthogonal Frequency Division Multiplexing (OFDM) is the transmission waveform used in NR. It is a way of transmitting data over multiple frequencies simultaneously (FDD), where the signals on the subcarriers are orthogonal to eachother. The symbols are modulated/demodulated by FFT, and the orthogonality of the signals cancel out the interference between carriers. This property of the waveform can be seen in Figure 3.3, where the three waves correspond to three subcarriers. It can be observed that the amplitude of the other waves is zero in the center of each peak. This leads to increased robustness in fading channel conditions, and also simplifies the transmitter and receiver design. The high spectral efficiency when using OFDM together with the simplicity of its implementation has made it a key technology in both LTE and NR.

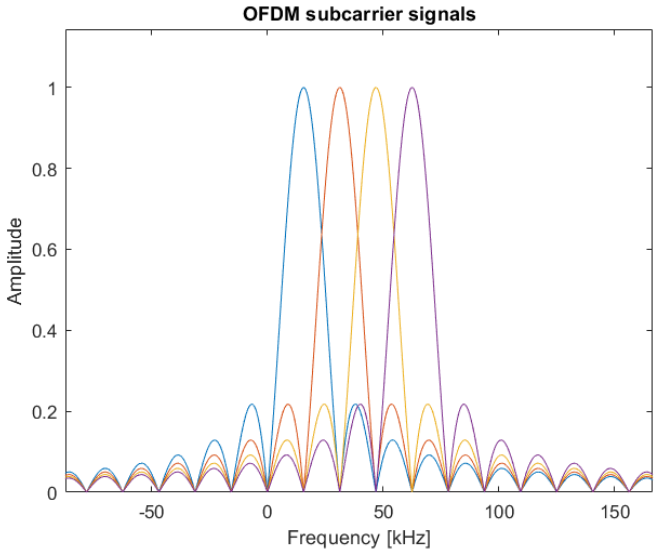

Figure 3.3: Waveform structure of OFDM modulation.

For the modulation to work properly, the orthogonality between subcarrier signals needs to be maintained or restored at the receiver. This puts pressure on synchronization and frequency offset estimation. Breaking the orthogonality be-

tween the subcarriers causes interference between the carriers and leads to high error rates. To increase the robustness of the modulation, cyclic prefix (CP) is introduced between symbols in the time domain. The cyclic prefix consists of a certain number of samples from the end of each OFDM symbol. This results both in a guard interval between OFDM symbols in time, which decreases inter symbol interference (ISI), but also makes the FFT valid. A signal propagating through a multipath fading channel can be seen as a convolution in time domain, and with the cyclic prefix that convolution becomes circular. A circular convolution in time domain is equivalent to multiplication in the frequency domain after performing DFT. This provides low complexity channel estimation in the frequency domain and is a great advantage of OFDM.

3.5 Reference Signals

Channel estimation is crucial in wireless communications, and becomes increasingly important with the use of multiple antennas and increasing bandwidths. When the bandwidth is small, the probability of the channel response being somewhat constant over the full bandwidth is much higher than when the bandwidth is large. The use of OFDMA is another factor that makes the channel estimation important, as the modulation requires that the orthogonality between subcarriers is maintained. To combat the challenge of efficient and accurate channel estimation, NR uses several different reference signals. Reference signals are pre-determined symbols at specified locations in the resource grid, known by both receiver and transmitter.

One important reference signal in NR is DMRS, which is used for demodulation of the symbols in both uplink and downlink. For PUSCH and PDSCH, the DMRS is mapped to the resource grid at early positions. This allows the receiver to perform the channel estimation and process the incoming data in real time, rather than having to record large blocks of data before demodulation. The symbols are generated as pseudo-random sequences. Using certain initiation values for the sequence generation allows transmission of several orthogonal DMRS signals in the frequency domain [7].

In addition to DMRS, the use of Phase Tracking Reference Signals (PT-RS) has been introduced in NR. They are increasingly important as the carrier frequency and bandwidth is increased, which leads to larger phase noise. For small bandwidths and certain MCS configurations, no PT-RS is transmitted. The sequences are mapped sparesly in frequency domain, but occur frequently in time domain.

The downlink channel state information reference signal (CSI-RS) is mapped to one RB for each antenna port used. It is configured separately for each device, and is a flexible way of sounding the signal where the location and density of CSI-RS is not fixed. The estimates are used to enhance the performance of the downlink

transmission, and are the basis of the uplink multi antenna precoding.

The uplink channel sounding is performed using sounding reference signals (SRS). The signal is spread over the subcarrier with a configurable density, and the structure is based on a *Zadoff-Chu* sequence. As they are to be transmitted from UEs, it is important that the sequence is efficient from a power amplification point of view. The Zadoff-Chu sequence is a phase rotated sequence with constant amplitude, which fills the efficiency requirement in the frequency domain. Another property is that the fourier transform of a Zadoff-Chu sequence is also a Zadoff-Chu sequence, and the sequence thus has a constant amplitude in the time domain aswell. The channel estimates are then used for the downlink precoding or beamforming [7].

3.6 Uplink and Downlink Transmission

The transmission of data over the Downlink Shared Channel (DL-SCH) starts with channel coding. If the data sequence is longer than the block size of the LDPC code used, the channel coding is initiated by dividing the sequence into multiple code blocks. Each code block is then appended with separate Cyclic Redundancy Check (CRC) bits. The blocks are encoded using an LDPC code, where the code rate is determined by a step referred to as Rate Matching. The resulting bitstream is then scrambled and modulated to complex symbols.

Through layer mapping, the symbols are distributed to different layers if the number of layers are larger than one. The Demodulation Reference Signal (DMRS) is then added to the designated resource blocks and precoded together with the PDSCH symbols. The precoding is where the symbols are mapped to antenna ports, after which a Channel State Information Reference Signal (CSI-RS) is added [2]. The signal is used by the UE to calculate the CSI that is reported back to the gNB in the uplink. The symbols are then mapped to available resource blocks and scheduled for transmission. They are also mapped to physical antennas, modulated with OFDM, upconverted to the desired carrier frequency and transmitted. The DL-SCH processing is illustrated in Figure 3.4.

Figure 3.4: DL-SCH processing steps [7]

Uplink transmission over the Uplink Shared Channel (UL-SCH) is very similar to that over DL-SCH. One difference is that the uplink supports DFT precoding and therefore one more modulation, namely $\pi/2$ BPSK. The CSI-RS signal is

replaced by a Sounding Reference Signal (SRS) [2]. The SRS is provided by the network and used at the gNB to estimate the channel properties. The UL-SCH processing can be seen in Figure 3.5.

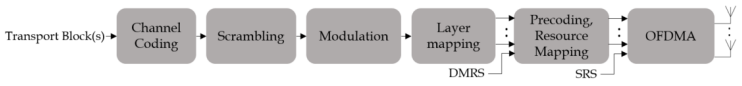

Figure 3.5: UL-SCH processing steps [7]

3.7 Duplex Modes

NR supports both Time Division Duplexing (TDD), where the same frequency resources are used for uplink and downlink communication, and Frequency Division Duplexing (FDD), where the communication is instead separated in the frequency domain.

To support the new use cases for 5G, defined in section 2, the TDD scheme has been designed to be dynamic. This means that the ratio between uplink and downlink transmissions can be changed when needed. This is important as it is becoming increasingly difficult to statistically predict the characteristics of uplink and downlink traffic in new types of connections [12].

When FDD is used, uplink and downlink communication is theoretically possible during the same time slot. Whether it can be carried out or not depends on if the UE has the functionality to do so within the current frequency band. The scheduler will then adapt the timing so that transmission and reception is not simultaneous for that particular UE [7].

Chapter 4

Wireless Channels

This section presents relevant theoretical concepts related to the wireless channel such as multipath propagation, diversity and noise. An understanding of these concepts is required before moving further into beamforming.

4.1 Small Scale Fading

When a signal is transmitted in an environment it will be reflected by surrounding objects such as walls, the ground, street signs and cars. Many of the reflected signals will end up at the receiver antenna, which in a single antenna system will simply add them together. The described scenario is illustrated in Figure 4.1. If each transmitted signal is denoted

$$s(t) = Re\{y(t)e^{j2\pi f_c t}\}, \tag{4.1}$$

where $y(t)$ is the baseband signal and f_c is the carrier frequency. Then the signal at the receiver can be expressed as a sum of the received signals from all paths as

$$r(t) = Re\{\sum_{n=1}^{N} \alpha_n(t)e^{-j2\pi\Phi_n(t)}e^{j2\pi f_c t}y(t-\tau_n)\}, \tag{4.2}$$

where $\Phi_n(t)$ is the phase of the nth received signal, α_n the amplitude of the nth signal and τ_n the time delay of the nth signal [15].

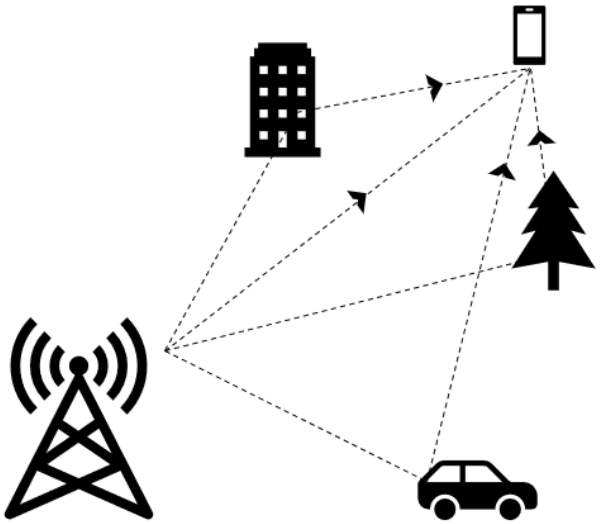

Figure 4.1: Multipath propagation.

This means that the different lengths of the propagation paths will cause the components of the received signal to have different attenuations and delays, and these multipath components can add upp either constructively or destructively. This phenomenon is called small-scale fading and is a major challenge in wireless communication systems [16].

4.2 Statistical Channel Models

The complexity of multipath propagation is often too high for deterministic models. The channel is therefore often described using statistical models. Which statistical model to use depends on the transmission scenario.

When there is no dominant multipath component, such as a Line-of-Sight (LOS) component, the expected amplitude of the received signal can be described by a Rayleigh distribution. The Rayleigh distribution is described by the cumulative distribution function (cdf)

$$cdf_{Rayleigh}(r) = 1 - e^{-\frac{r^2}{2\sigma^2}}, \tag{4.3}$$

where $2\sigma^2$ is the root mean square (rms) value of the distribution [16]. The model

is widely used as it is a good model for most scenarios where there is no LOS, and even when there is a dominant component it is a good measure of the worst case scenario. Furthermore the model is very simple and easy to use [16]. In the NLOS scenario, the phase is a sum of multiple random variables assumed to have no bias. The phase can therefore be modelled by a uniform distribution.

In the case that there is a dominant component, such as a LOS scenario, the Rician fading model can be used for modelling the amplitude. The relation between the LOS component power and the average power of the other components can then be used to weight the mean square value of the distribution. The cdf for a Rice distribution is

$$cdf_{Rice}(r_m) = \int_0^{r_m} \frac{r}{\sigma^2} e^{-\frac{r^2+A^2}{2\sigma^2}} I_0\left(\frac{rA}{\sigma^2}\right) dr, \tag{4.4}$$

where $\frac{A^2}{2\sigma^2}$ is the ratio between the LOS component power and the power of the other components, also called the $Ricefactor$, and I_0 is the Bessel function of order zero. Due to one component having a greater impact on the received signal, the phase can no longer be modelled by a uniform distribution but requires a more advanced modelling [16].

4.3 Large Scale Fading

Another type of fading in wireless channels is large scale fading. This is also referred to as *shadowing* as it is caused by obstruction of the signal by large objects, such as buildings. This type of fading is changing much slower over time than the small scale fading, and reduces the received signal power significantly [16]. As illustrated in Figure 4.2, the effect of the large scale fading is present as long as the UE is located in the shaded area. The signal that reaches the UE consists of reflected signals from other surrounding objects.

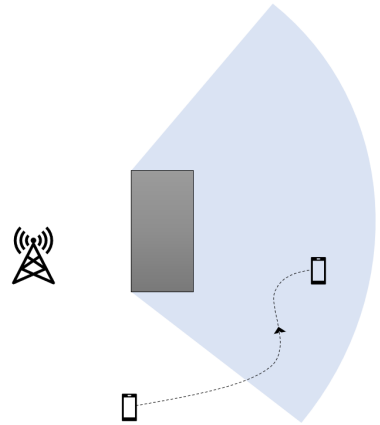

Figure 4.2: *Large Scale Fading* or *Shadowing* caused by a UE moving behind a building.

4.4 Path Loss

A signal propagating in free space will be subject to attenuation in the form of path loss. The path loss depends on the surroundings, type of antenna, directivity of antenna and other factors, but is often estimated using *Friis Law*. The expression for the expected received power is then

$$P_{rx} = P_{tx}\Big(\frac{\lambda}{4\pi d}\Big)^2, \tag{4.5}$$

or in dB scale

$$P_{rx} = P_{tx} - 20log_{10}\Big(\frac{4\pi d}{\lambda}\Big), \tag{4.6}$$

where P_{rx} is the receive power, P_{tx} the transmit power, λ the wavelength and d the distance between receiving antenna (Rx) and transmitting antenna (Tx). It assumes omnidirectional antennas, antennas transmitting the same power in all directions, and a small bandwith. The formula is only valid when assuming free space transmission and *far field conditions*, meaning that the distance between Rx and Tx is large enough. More specifically, the far field region is where

$$d > \frac{2D^2}{\lambda}, \tag{4.7}$$

where d is the distance between Rx and Tx, D the largest dimension of the antennas and λ the wavelength [16]. In multipath propagation, each path will be subject to a path loss depending on the distance of that specific path. Longer paths will thus arrive with lower power than shorter paths.

4.5 Noise

In addition to fading, the signal is also subject to noise. There are different types of noise, one of them being thermal noise. Thermal noise is caused by the temperature of the enviromnent and the bandwidth of the spectrum. The noise power at 27 °C is

$$P_n = N_0 B, \tag{4.8}$$

where $N_0 = -174$ dBm/Hz and B is the bandwidth of the receiver. Other types of noise are man made noise, which is noise caused by other electrical equipment, and receiver noise, which is noise caused by the receiver side amplifiers. The total noise at the receiver is obtained by combining all noise components.

4.6 Diversity

The idea of diversity is to transmit the same information over several statistically independent channels. Using multiple antennas increases the spatial diversity of the system by allowing the same signal to propagate over several (ideally) independent channels between the antenna pairs, and the angular diversity by receiving the same signal from different positions. Another way of increasing diversity is to transmit the same signal over more than one frequency, which is known as frequency diversity.

The signals can then be used or combined at the receiver using different methods. The simplest method would be not to combine them but to choose the signal at the antenna with the highest Signal to Interference plus Noise Ratio (SINR). This generally increases the SINR at the receiver, as the probability of the signal at one antenna having a sufficient SINR increases with a more antennas, and therefore leads to a much lower outage probability.

4.7 Channel Estimation

As mentioned in section 3.5 about reference signals, channel estimation is extremely important as wireless channels are frequency selective and also change over time. One way of estimating the channel is to insert known sequences of data in the transmitted signal. NR uses such pilot aided estimation in the frequency domain by mapping reference symbols, CSI for downlink and SRS for uplink, to the resource grid.

The symbols are mapped with certain spacing in frequency and time domain. An example of SRS mapping in the resource grid is shown in Figure 4.3. The

spacing in frequency can be either 2 subcarriers as in the figure, or 4 subcarriers. The known transmitted symbols are used for channel estimation by dividing the received symbols with the known transmitted symbols, and interpolating the achieved matrix for the rest of the resource grid. The received symbols can then be equalized by dividing them with the estimated channel matrix according to

$$H_{est} = \frac{p_{received}}{p_{transmitted}}, \tag{4.9}$$

$$X^* = \frac{X}{H_{est}}, \tag{4.10}$$

where p denotes the pilot symbols, X is the received resource grid and X^* the equalized received symbols to be decoded.

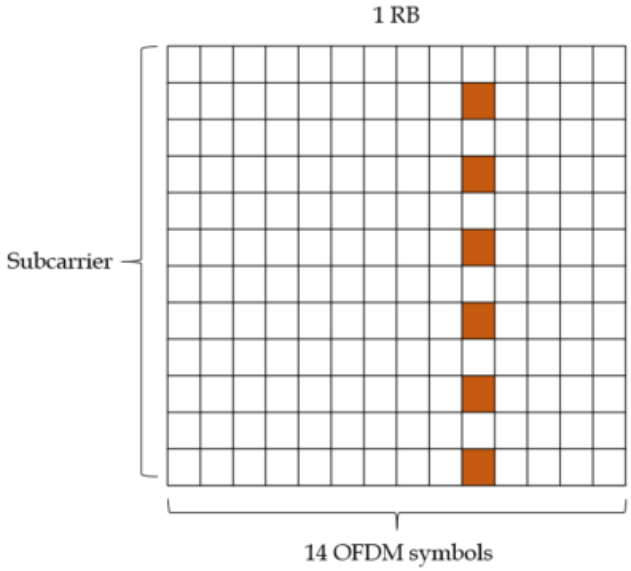

Figure 4.3: SRS mapping with a spacing of 2 subcarriers in the frequency domain.

4.8 Characterization of Frequency Response

A channel that varies in the frequency domain is called a frequency selective channel. This is normally the case in real world wireless transmissions, and is an important reason to why the pilots need to be spread out over the subcarriers. The pilots provide an estimation of the channel frequency response, which can be used to equalize the received signal in order to lower the bit error rate (BER).

However, sometimes the characteristics of the frequency response can be of certain interest.

The channel impulse response gives a measure of how the channel responds to a dirac pulse in time domain. It can be obtained by the inverse fourier transform of the channel estimation matrix as

$$h(\tau) = \int_{-\infty}^{\infty} H_{est}(f) e^{j2\pi f\tau} df, \tag{4.11}$$

From the channel impulse response, the power delay profile can be determined. It is given by

$$PDP(\tau) = |h(\tau)|^2, \tag{4.12}$$

and can in turn be used to obtain the mean delay of the multipath components as

$$\tau_{mean} = \frac{\int_0^{\tau_{max}} \tau PDP(\tau) d\tau}{\int_0^{\tau_{max}} PDP(\tau) d\tau}. \tag{4.13}$$

The PDP and τ_{mean} can finally be used to determine the root mean square (RMS) delay spread [22] as

$$\tau_{rms} = \sqrt{\frac{\int_0^{\tau_{max}} (\tau - \tau_{mean})^2 PDP(\tau) d\tau}{\int_0^{\tau_{max}} PDP(\tau) d\tau}}. \tag{4.14}$$

The delay spread is essentially a measure of how the multipath propagation affects the transmitted signal. A large RMS delay spread means that the multipath components arrive at the receiver with very varying delays. The delay spread is a time domain characteristic but is directly related to the coherence bandwith, which is a frequency domain measure. The coherence bandwidth is the bandwidth during which the fading can be considered flat. If the coherence bandwidth is smaller than the transmission bandwidth, frequency selectivity is observed. There are different ways of obtaining the coherence bandwidth, and one proposed relation is

$$B_c = \frac{1}{\alpha \tau_{rms}}, \tag{4.15}$$

where B_c is the coherence bandwidth, τ_{rms} the RMS delay spread and α a constant depending on the PDP of the channel [27].

Another method to measure these parameters is the level crossing rate, LCR, which measures the number of times the frequency response crosses a certain amplitude in the positive direction [26]. The LCR can be used to calculate τ_{rms}, and to determine the average bandwidth of fades (ABF). The average bandwidth of fades is a measure for the average bandwidth that the frequency response is below a certain threshold. ABF is another measure of how volatile the frequency response is. LCR is a very simple and fast way to determine the parameters, however it suffers severe drawbacks when the signal is subject to noise [25]. Figure 4.4 shows

how the noise severely affects the LCR of the frequency response. The impact could be reduced to some extent by appropriate low pass filtering.

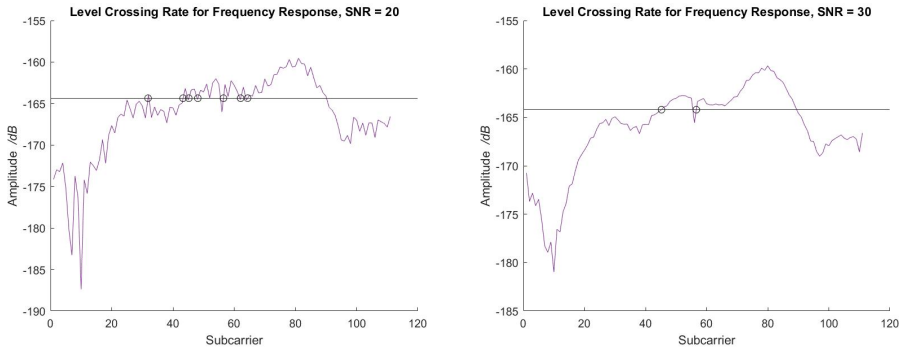

(a) SNR = 20 **(b)** SNR = 30

Figure 4.4: Level crossings for the same channel with different levels of noise.

A less noise sensitive way to find the coherence bandwidth of the channel is the frequency correlation function

$$R_H(\Delta f) = E\{H(f)H^*(f + \Delta f)\}, \tag{4.16}$$

which is essentially the expected value of the correlation between the frequency response at frequencies f and $f + \Delta f$ [5].

The correlation function is also the IFFT of the PDP. The coherence bandwidth is then equal to the smallest Δf where $R_H(\Delta f)$ is below a certain value. It is common to define different coherence bandwidth levels such as $B70$ and $B90$, see Figure 4.5, which are defined as the Δf where the frequency correlation function is below 0.7 and 0.9 respectively.

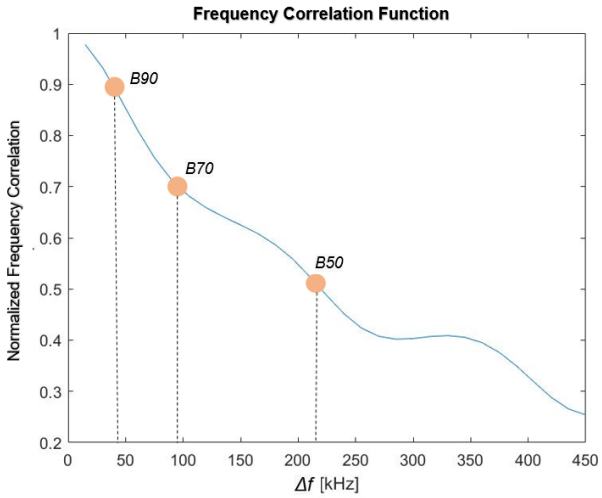

Figure 4.5: $B90$, $B70$ and $B50$ for a frequency selective channel.

Chapter 5

Downlink Beamforming in NR

This section introduces the concept of MIMO, using multiple antennas to achieve better performance during transmission. Making good use of a large number of antennas requires understanding of the benefits and possibilities of the technique. First, the general idea and benefits of MIMO are discussed, after which the concept of precoding is introduced together with three different linear precoding techniques.

5.1 MIMO

The concept of MIMO, Multiple-Input Multiple-Output, is to use an array of transmitting and receiving antennas instead of using a single Tx-Rx antenna pair. There are many benefits of this technology. One benefit is the increased angular diversity, which gives the opportunity to reduce the impact of destructive multipath interference [16].

Another possibility that opens up with multiple antenna systems is increased directivity of the signal. Using the channel estimates from the uplink reference signals, the signal from the antenna array can be directed towards the location of the receiving user equipment (UE), or towards the gNB using the downlink reference signals. This increases the received power at the UE location without increasing the transmit power, and further opens up for multiple users sharing the same frequency and time resources using spatial multiplexing. Directing the signal from the base station to a user in the network is known as beamforming. Finally, MIMO can also be used for spatial multiplexing to increase the spectral efficiency by transmitting several data streams in the same frequency band.

Single user MIMO (SU-MIMO) can be used to increase the signal strength at the user, which also extends the range of the signal. With the higher frequency bands of 5G NR, this is an important technique to combat the large path losses.

Multi user MIMO (MU-MIMO) is where the spatial multiplexing can be deployed by directing beams towards different users. How many users that can share the same resources depends on how many uncorrelated channels there are in a certain scenario. This depends on the environment, number of antennas and the location of the UEs. The extra resources in the spatial domain are often referred to as *layers*, and the maximum layers is the smallest number of antennas used for the transmission at the UE and BS. MU-MIMO requires much more precise channel knowledge to get a good performance, as the interference will otherwise be very strong.

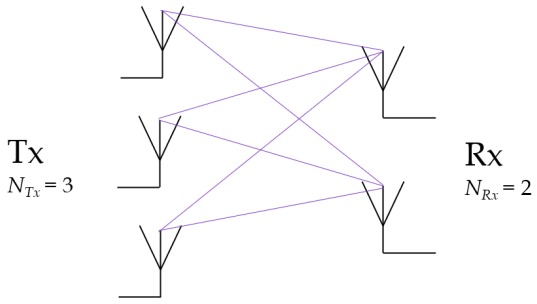

Figure 5.1: 3x2 MIMO system.

Figure 5.1 shows a 3x2 MIMO system and the LOS paths between all antenna pairs. Each path will have a different path loss and be exposed to different scattering effects. The channel matrix for a MIMO system can therefore be written as

$$H = \begin{bmatrix} h_{1,0} & h_{1,1} & \dots & h_{1,N_t} \\ h_{2,0} & h_{2,1} & \dots & h_{2,N_t} \\ \vdots & \vdots & \vdots & \vdots \\ h_{N_r,0} & h_{N_r,1} & \dots & h_{N_r,N_t} \end{bmatrix}, \tag{5.1}$$

where N_r is the number of receiver antennas and N_t the number of transmitter antennas. Each element in the channel matrix corresponds to the impulse response of the channel between an antenna pair. This means that $h_{i,j}$ denotes the channel impulse response of the channel between the ith receiver antenna and jth transmitter antenna [16].

There exists one channel matrix for each symbol in the resource grid. For one frame consisting of 14 OFDM symbols and 180 subcarriers, there will be $14 \times 180 = 2520$ different channel matrices.

5.2 Precoding

Precoding is one of the last steps before transmitting a signal over the physical channel. It is the step where the transmitted symbols are weighted to create the desired effect of directivity. For downlink beamforming, the weights are calculated based on the CSI from the uplink and there are several different precoding techniques. These techniques can be categorized as either linear or non-linear, where the linear techniques are usually preferred in practice as their complexity is relatively low in comparison to their performance [4]. The goal with precoding is to multiply the symbol stream with appropriate weights according to

$$y = Wx, \tag{5.2}$$

Where x is the initial symbol vector, W the $N_{TX} \times N_{RX}$ weight matrix and y is the weighted vector to be transmitted.

5.2.1 Linear Precoding Schemes for Downlink Beamforming

As previously stated, linear precoding algorithms are commonly used in downlink beamforming due to their high performance and low complexity. They all use the downlink channel matrix H, which is the transpose of the uplink channel matrix when the channel is assumed to remain constant during the time between UL and DL transmission. This section presents three different linear algorithms for obtaining the weight matrix W.

5.2.2 Maximum Ratio Transmission

Maximum Ratio Transmission (MRT) can be considered the simplest algorithm for MIMO precoding. The weight matrix is given by

$$W = H^H, \tag{5.3}$$

where W is simply the hermitian (conjugate transpose) of the channel matrix. The technique is also referred to as Matched Filter precoding and aims to maximize the SNR at the receiver [24].

5.2.3 Zero Forcing

Zero Forcing (ZF) ideally cancels the interference between users, increasing the system performance and possibly allowing for spatial multiplexing. The weight matrix is given by

$$W = H^H(H^T H^H)^{-1}, \tag{5.4}$$

In the theoretical event that the CSI is known and there is no additive noise, the performance of ZF is very close to capacity, however the algorithm performs significantly worse in high SNR [9]. Imperfect CSI also degrades the performance since the signal cannot be perfectly cancelled at other users, leading to interference. The efficiency of the nullification is also dependant on the correlation between the user channels, where less correlated channels result in higher capacity [10]. The algorithm requires the number of transmit antennas to be larger than the number of UEs, and yields best results when the number of transmit antennas is significantly larger than the number of UEs [18].

5.2.4 Regularized Zero Forcing

Regularized Zero Forcing (RZF) is an enhanced version of ZF to account for scenarios where there is additive noise and imperfect knowledge of the CSI. This is the case in real world applications, making the RZF a useful precoding technique. The weight matrix is given by

$$W = H^H(H^T H^H + \alpha I)^{-1}, \tag{5.5}$$

where α is the normalization factor which can be optimized with regards to different parameters, commonly the noise variance. RZF does not completely cancel the inteference between users, but reduces it while taking the noise into account [18]. When α represents the noise variance of the system, the precoding technique becomes MMSE precoding. MMSE does not completely cancel out interference between users, but instead minimizes the overall error between receive and transmit signal by taking the noise into account. This results in a tradeoff between interference nulling and power efficiency [10].

5.3 Equalization and Combining

As described in section 4.7, channel estimation in single antenna systems is done by dividing the received symbols with a channel estimate. In MIMO, one can instead make use of the multiple antennas in the equalization. One important technique for equalization is Zero Forcing, which just as for a single antenna system multiplies the received symbols with the channel inverse. The difference is that when the equalized symbols from each receive antenna are added together, the impact of the noise is reduced.

The received signal y can be denoted as

$$y = Hx + n, \tag{5.6}$$

where H is the MIMO channel matrix and x the transmitted signal. x can then be estimated by

$$x = (H^H H)^{-1} H^H y, \tag{5.7}$$

the ZF equalized x symbols can then be decoded in the same way as for a single antenna system [23]. The number of symbol streams x is equal to the number of layers used for transmission, and the symbols from each layer needs to be mapped to the correct data locations.

5.4 Application in 5G NR

Beamforming is, as previously described, a crucial technology in 5G NR. The techniques described above are used in *digital beamforming*, meaning that the baseband symbols are weighted before it is converted to an analog signal. Another type of beamforming is *analog beamforming*, where the phases of the RF signals are changed to form a beam. This happens in the RF domain, and limits the beamforming to one beam per antenna array. The phases are applied using a codebook, where each code is a set of phase shifts for the signals to each antenna that results in a certain beam pattern [17]. In mmWave, the higher frequency regions of NR, it is expected that a combination of the techniques will be used. It is referred to as *hybrid beamforming*, and is performed by first weighting the baseband symbols by precoding and later also applying the analog beamforming. The combination of both is a promising solution to the path loss issues of higher frequencies.

Chapter 6

Adaptive Frequency Resolution Algorithm

One large issue in telecom product development is shortage of computational resources. In a base station, the computations are typically distributed over a limited number of DSPs. As the complexity grows, which it certainly has with the later generations of mobile networks, the demand for these resources increases drastically. Shortage of DSPs can lead to bad timing and longer execution times. Anywhere where the complexity of the computations can be reduced is a possibility to optimize, speed up and make the real time system more robust.

The beamforming precoding, such as RZF described in section 5.2.4, consists of calculations where the inverse of a matrix is to be computed. This is a time consuming task, and if the number of times it needs to be executed can be reduced, resources can be saved. The aim of the frequency selection algorithm is therefore to reduce the frequency resolution of the beam weight calculations in a smart way where the BER is not heavily affected.

Furthermore, the algorithm needs to be simple so that it actually results in a lower complexity. If the algorithm is too extensive, there is a risk that the overall execution time is not reduced or even prolonged. This would happen if the execution time of the algorithm is longer than the time saved on the beamforming weight calculations.

In beamforming application, the channel estimates are commonly downsampled to PRB resolution. This means that there is only one channel estimate for each PRB, even though each PRB consists of 168 REs. These estimates are used to calculate the beamforming weights, and updating the weights every second PRB has been found good enough in most cases. In many cases, this is an unnecessarily high resolution resulting in a waste of resources. The goal is to implement a resolution selection algorithm that predicts how many PRBs can use the same beamforming weights without a significant increase in BER.

6.1 Adaptive Resolution

As a first step, it was decided that the algorithm should have four different resolutions to choose from, where each resolution is represented by a value n. The n-value is the inverse of the resolution, which can be seen in Table 6.1. As $\gamma = 2$ is used in the product today and shows good performance, $\gamma = 1$ was not considered an option. It could be possible to add even lower resolutions, but the limit was set to $\gamma = 16$ for this thesis.

γ [PRB]	Weight calculations per PRB
2	1/2
4	1/4
8	1/8
16	1/16

Table 6.1: Possible resolutions for the algorithm to choose from.

Figure 6.1 illustrates how the processing resolution can be changed adaptively over time on a slot basis. The colored PRBs represent the weight updates which occur with the granularity to be set by the algorithm. In the figure, the third slot allows for a lower resolution due to a less frequency selective channel, and the first slot requires a higher resolution.

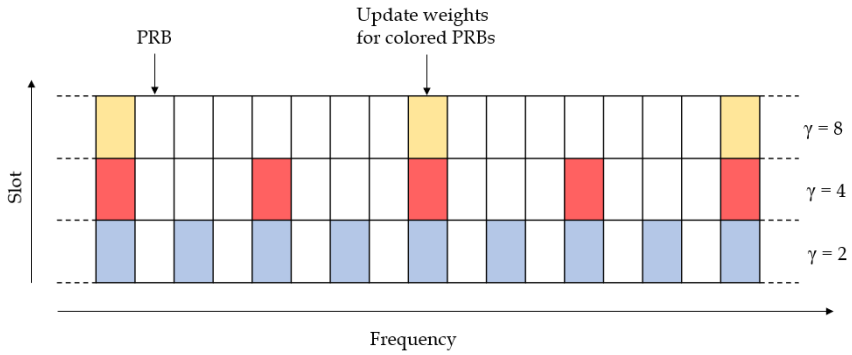

Figure 6.1: Frequency resolutions assigned per slot.

Two different optimization criterions are to be explored in the thesis, resulting in two different algorithms. One is to choose the lowest resolution possible while maintaining the BER near that of 2 PRB resolution. The other should choose the lowest resolution possible while keeping the BER below a pre-defined threshold.

The main factor that will determine how frequent the beamforming weights need to be updated in the frequency domain is the frequency selectivity of the channel, that is, how much the channel varies over the frequency spectrum. In section 4.8, average bandwidth of fades, rms delay spread and coherence bandwidth were presented as measures for the frequency selectivity of the channel.

For the first version of the algorithm, the selected parameter was calculated and used for the resolution selection. All three parameters were evaluated separately to see which one was best suited to use in the algorithm. To do this, suitable thresholds were first estimated. This process is presented as a separate simulation in section 7. Figure 6.2 shows a high level overview of the frequency selection algorithm.

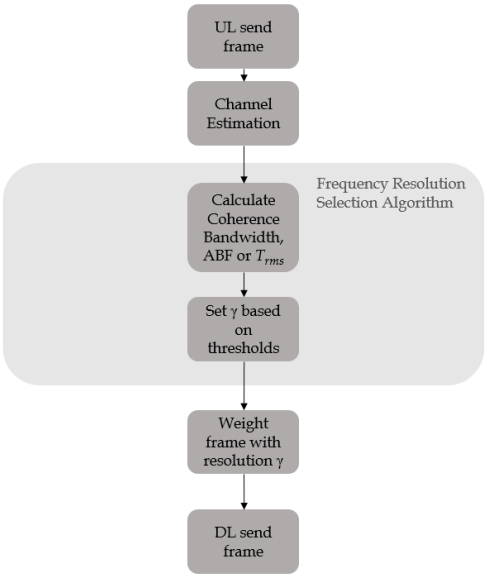

Figure 6.2: Frequency resolution algorithm.

In the second version, only the BER is measured and the resolution adapted depending on wheather the BER is above or below the set threshold. The main focus of the thesis work is on the more advanced algorithm previously presented, but this BER limit algorithm is presented as a simple alternative. Figure 6.3 shows an overview of the algorithm in the simulation scenario.

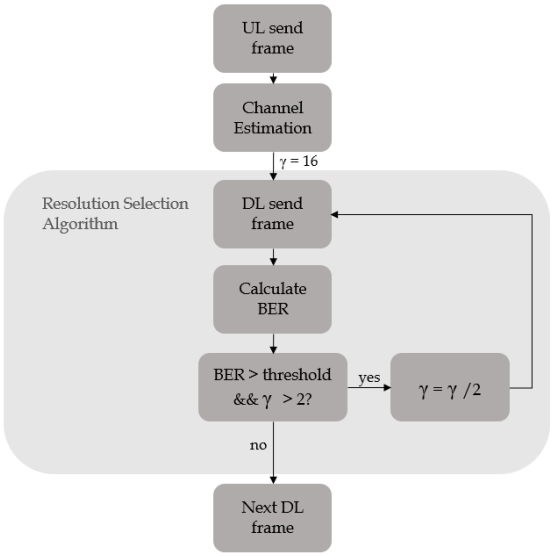

Figure 6.3: BER limit resolution algorithm.

Chapter 7

Methodology

The algorithm was developed and tested through incorporation in a Matlab simulation model. The simulator was originally built for LTE, and re-organized for NR in 2020 by master thesis student Juan Guirado Puigcerver [11]. The basic functionality for the transmission chain was re-used, however new simulation scenarios were constructed along with incorporation of the algorithm. Improvements were also made to the simulation where needed, and errors were corrected as they emerged. This section presents the building blocks of the simulator and the scenarios constructed for this project.

7.1 Basic Simulation Flow

The simulation transmits data divided into frames and is designed for a certain transmission flow. Before any data is to be transmitted, the channel is constructed. This means the channel matrix for each antenna pair is created according to a statistical channel model. The channel model Winner 2 is used in the simulator, which is a spatially coherent stochastic channel model for MIMO systems. It is provided by the Matlab Communications Toolbox, and is valid for multiple channel parameters such as delay spread, angle of arrival and cross-polarization. The fading model used can be either Rician or Rayleigh fading depending on the LOS/NLOS option and the different pre-defined layout scenarios for the model [13]. The parameters given by the model are the channel matrix H, which is the channel matrix between each antenna pair, and the path delays.

When the channel is created, the idea is to start with sending uplink frames where PUSCH-data and SRS symbols are mapped to the resource grid. The uplink transmission then consists of layer mapping, OFDMA modulation, upsampling, upconversion, and power normalization. The beamforming is only performed in the downlink, and the precoding step described in section 3.6 is therefore left out

for uplink. The signal is then stepped through the channel one subframe at a time according to the created channel. This means that the signal is multiplied with the channel matrix H, and that the signals subject to path delay are summed up at the receiver.

Channel estimation from the uplink SRS symbols is performed when the signal is received. The procedure is described in section 4.7 and linear interpolation is used. When the channel estimation is obtained, the uplink signal can be decoded and the BER calculated. In this simulator however, the main focus is the downlink beamforming. Therefore decoding the uplink signal is often discarded in order to save time, but can be a great asset when debugging as the transmission chain is simpler than the downlink since it excludes the precoding.

Instead of calculating the BER for uplink, the simulations often proceed to directly transmit the downlink frames. The downlink transmission chain is very similar to the uplink, with multi antenna precoding added. The precoding is where the uplink channel estimations are used to perform the beamforming. The downlink channel matrix is the transpose of the uplink one if the channel is considered stationary within the time interval, and the different precoding techniques implemented in the simulator are MRT, ZF and RZF/MMSE. These are all described in section 5.2.

The signal is then once again stepped through the channel, and the received reference symbols are used for channel estimation. The final step is to decode the downlink data symbols to obtain the bit error rate, after which the overall results can be calculated. The simulation model is only implemented to support TDD, that is, the uplink and downlink transmissions are separated in the time domain.

A detailed view of the simulation flow can be seen in Figure 7.1, where the simulation starts with the uplink transport block, and the channel estimation from uplink transmission is used for downlink precoding. The resolution selection algorithm is not included in the block diagram.

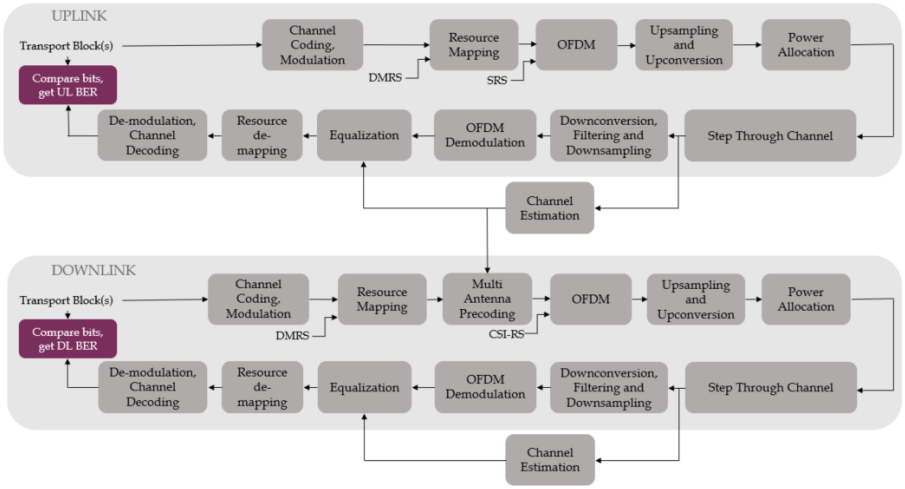

Figure 7.1: Block diagram of the simulations.

7.2 Simulation Scenarios

For the results to be as useful as possible, the simulations must resemble a real world scenario. This section presents the setup for the simulation runs in the project. As the purpose of the different simulations are different, so are the parameters and layouts. The first simulation is designed to evaluate the correlation between frequency response parameters of the channel and the optimal resolution. The results from the first simulation determine the thresholds for the adaptive resolution algorithm. The next simulation evaluates the performance of the algorithm when using the decision boundaries decided in the first simulation. The third simulation shows the chosen resolutions for two different UEs in the same layout using MU-MIMO. Finally, the BER limit algorithm is evaluated.

The layout scenario for the winner II channel model was set to B1 - Urban Micro Cell - for all simulations. The channel for the B1 scenario is modelled with the assumption that the base station is located below the top of surrounding buildings [13]. As many of the new deployment scenarios of 5G will operate at shorter distances between gNB and UE due to the higher carrier frequencies, this scenario can be viewed as a good representation for an urban scenario. The positions of the UE and gNB are static throughout the simulations, while the SNR is stepped through the specified interval.

The gNB is equipped with 64 antenna elements with half a wavelength spacing. Any UE has one antenna, and the scenario is thus Multiple Input - Single Output (MISO) for the SU-MIMO case.

7.2.1 Multiple Resolutions Simulation

The basic SU-MIMO setup was created by placing one UE at position [0,0] and a gNB at [200,200] in a grid as shown in Figure 7.2, which gives a distance of 282 meters. Other parameters used were

- Bandwidth: 20 MHz
- Carrier Frequency: 24 GHz
- Modulation: QPSK
- Numerology: 0
- Number of subframes: 5
- Precoding technique: MMSE
- Number of gNB antennas: 64
- Number of UE antennas: 1

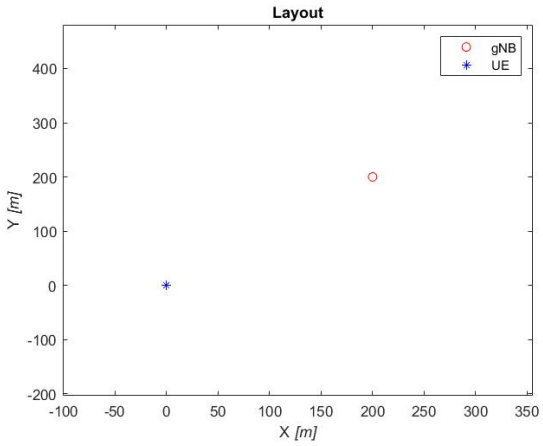

Figure 7.2: Layout of simulation.

To understand how the BER was affected by the resolution, a simulation that tested all possible resolutions was created. The SNR range was set to (0,30) [dB] with a granularity of 5 dB. The simulation flow described in section 7.1 was run for the different SNR levels, once for each frequency resolution γ. The BER was then plotted for each γ-value to clearly display the impact of the resolution. The ABF, T_{rms} and coherence bandwidth of the channel were calculated from the frequency response for the highest SNR of each resolution, in this case 25 dB. The average total runtime of weight calculations was also measured for each resolution.

As the purpose of this simulation was to estimate the suitable resolution for each channel, it was run for 200 different channels. The BER plots, ABF, T_{rms} and coherence bandwidths were saved for each channel. The ABF and coherence bandwidths were calculated on a PRB basis. The plots were then categorized into suitable n-values, depending on how the BER was affected by the resolution. A resolution was accepted if the average increase of BER over the SNR range was under 10% on average. This means that the increase of BER can be higher than 10% for some SNRs, and the resolution is still accepted. The selected resolutions could then be plotted together with ABF, T_{rms} and coherence bandwidth respectively to see if any correlation could be found. Examples for four different channels, with different optimal resolutions, is shown in Figure 7.3.

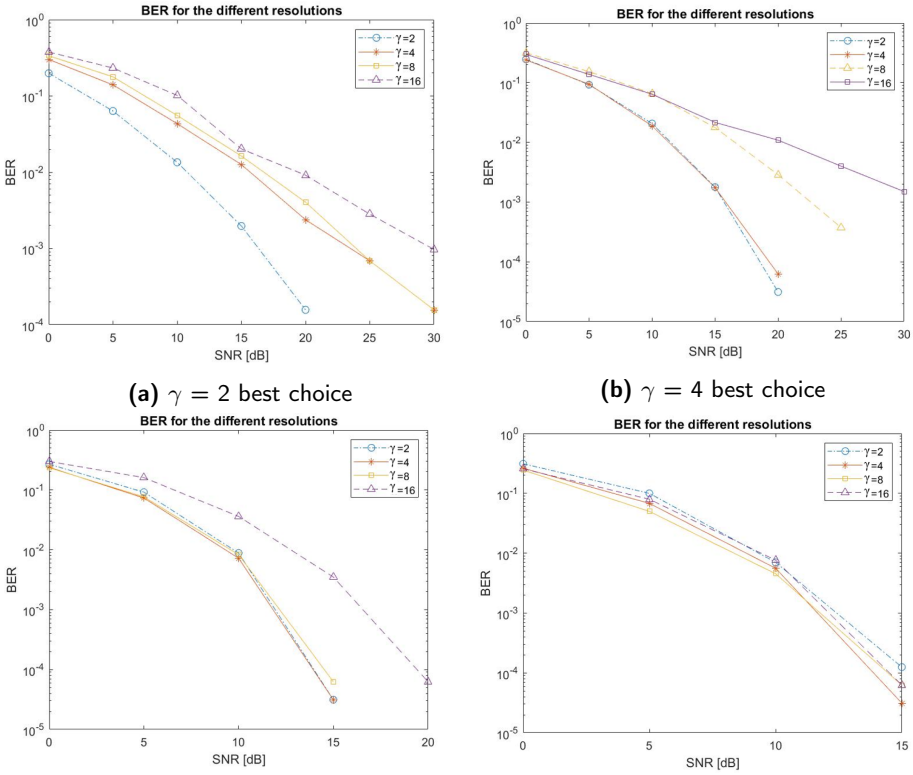

(a) $\gamma = 2$ best choice

(b) $\gamma = 4$ best choice

(c) $\gamma = 8$ best choice

(d) $\gamma = 16$ best choice

Figure 7.3: BER plots for four channels where the resolutions $\gamma = 2, 4, 8, 16$ can be found suitable.

The ABF and coherence bandwidths were calculated as described in section 4.8, where the coherence bandwidth was determined using the absolute value of the frequency correlation function. Estimating T_{rms} required more analysis as the impulse response and power delay profile were estimated through IFFT of the channel matrix in the frequency domain. As can be seen in Figure 7.4, there is a

noise floor at around -33 dB. To estimate the delay spread, this noise floor needs to be removed. This can be done by setting a threshold above the noise floor and removing everything below the limit. If the noise is not removed, the delay spread estimation will be off, as noise will then be taken into account as multipath components. As the threshold can be set to -33 dB, or -30 dB to gain some margin to the noise floor, all multipaths that arrive with an attenuation of -30 dB or lower will be discarded as noise. As components arriving with such low relative power will have little impact, it can be seen as enough for this project to ignore them and estimate T_{rms} with a threshold of -30 dB. The equations for the T_{rms} calculations can be found in section 4.8.

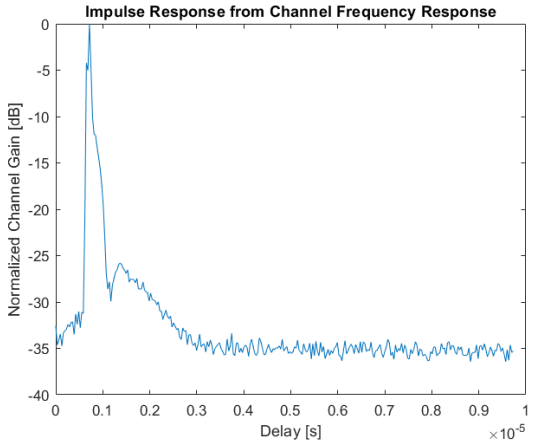

Figure 7.4: PDP from frequency response

7.2.2 Adaptive Resolution Simulation

The adaptive resolution algorithm was incorporated after suitable thresholds were estimated. The simualtion was then run with the same parameters and layout as the previous simulation (section 7.2.1), and consisted of two runs over the SNR range (0,30) [dB]. The first run was done with a resolution of 2 PRB, the resolution used as reference for BER, and the second one with adaptive resolution. The total BER could then be compared between the two scenarios to evaluate the performance. The average weight calculation runtime was measured, and the average chosen resolution was calculated.

The matlab functions **tic** and **toc** were used to measure the runtime. This step proved to be difficult as the calculations were in the millisecond range, and when measuring the full beamforming runtime they did not have noticeable impact. When measuring only the weight calculations, the runtime results were very inconsistent. As the weight calculation runtime should decrease linearly with the resolution, the average chosen resolution was determined to be a better measure

for resource saving than the runtime measured by matlab.

ABF, T_{rms} and the most suitable decision paramter for coherence bandwidth, with the thresholds found from the previous simulation, were used for the decision making. Only one variable was used at a time, and the simulation was run 100 times for each of the measures as decision parameter. The increase of BER was recorded and compared with the BER of 2 PRB resolution in the same channel. The aim was to explore the pros and cons of the decision parameters and decide which one would be better suited for further development.

As the results depended on the selected channels, the same channels was generated for all simulation runs. This was accomplished by generating a vector of random numbers and using the values as seeds for the Winner II channel generator. AWGN was still generated separately for each simulation.

The average increase of BER was calculated per SNR and then averaged over the SNR range. The fluctuations of BER in higher SNR ranges was expected to be larger than those in lower SNR. The reason for this is that there were fewer errors, and small variations in the number of errors resulted in relatively large changes in BER. This could be avoided by running the simulation for an extremely large amount of bits, however that would not be feasible to do on a regular computer as the simulations were already very time consuming.

7.2.3 Number of Antennas Dependence

To evaluate how the performance changed when using different numbers of antennas, the simulations for estimating thresholds and evaluating the algorithms were run for 8, 16, 32 and 64 BS antennas. The decision parameter used was T_{rms}, as previous simulations indicated it was the best suited parameter for resolution selection.

7.2.4 MU-MIMO Simulation with Two Users

To test how the resolution affected the BER in a MU-MIMO case, another simulation scenario was created. Two users were placed in [0,0] and [270,200], with the gNB in [200,200], thus using the layout shown in Figure 7.5. The two users were well separated from each other to reduce the correlation between the channels of the two users. To clearly see the impact of the resolution on the BER, the regular simulation flow was run in the SNR range [0,30] dB for four resolutions. The resolutions were initially set to $\gamma = 2, 4, 8, 16$ PRB, however they did not yield the desired performance. To successfully cancel out interference between the beams, MU-MIMO demanded a much more precise knowledge of the channel than SU-MIMO. Therefore the lowest resolution for this simulation was set to one RE.

As one PRB spans 12 x 14 = 168 REs, and the lowest resolution considered for SU-MIMO was two PRBs, the highest resolution run in this simulation was significantly higher than other resolutions previously considered. This is not feasible from a product development point of view as the computational resources needed for increasing the resolution from 2 PRB to 1 RE would be increased by 336 times.

The simulation was run for the resolutions $\gamma = 1$ RE, 1 PRB, 2 PRB, 4 PRB, after which their respective BER curves could be plotted together.

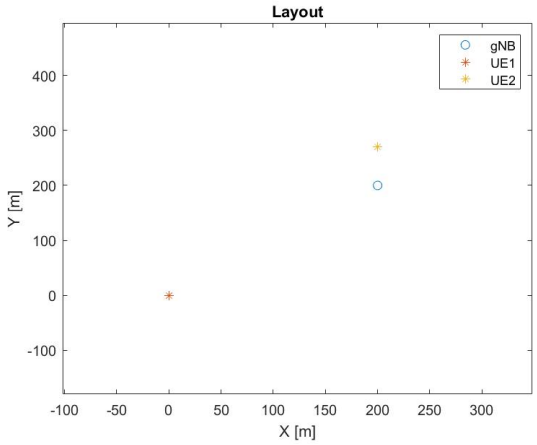

Figure 7.5: Layout of simulation.

7.2.5 BER Limit Algorithm Simulation

The second version of the algorithm, the BER limit algorithm, was designed to select the lowest possible resolution while keeping the BER under a threshold. The simulations were run with the same parameters and layout as the initial simulation in section 7.2.1, but with the BER limit algorithm incorporated. The simulation was run for the resolution 2 PRB, after which the adaptive resolution was run for each SNR of the same channel. The BER for the two simulations was saved and compared. The chosen resolutions were also saved for evaluation.

The simulation was run for 100 channels to evaluate the average performance where 10^{-1} and 10^{-2} were used as BER limits.

Chapter 8

Results and Discussion

This section presents the results of the different simulations described in section 7. Section 8.1 presents the threshold estimation for ABF, T_{rms} and coherence bandwidth resolution selection. The thresholds were then used for the algorithm decision making, and the performance of the algorithm with the different thresholds is presented in section 8.2. Section 8.3 presents the performance of the algorithm with different numbers of antennas. Section 8.4 presents an MU-MIMO scenario, and section 8.5 the results for BER limit version of the algorithm.

8.1 Multiple Resolutions Simulation

The plots for the relationships between resolution and ABF, $B90$, $B70$ and $B50$ can be seen in Figure 8.1. In the $B50$ plot it can be observed that the coherence bandwidth values for $\gamma = 2$ were consistently low, while the resolutions $\gamma = 4, 8, 16$ were harder to distinguish. The pattern was clearer for $B70$, where only $\gamma = 8, 16$ were fully overlapping. The most visually clear pattern would however be the $B90$, where no resolution levels were fully overlapping.

The noise sensitive ABF measure also displayed some visual correlation with the resolution. The main part of the data points were however overlapping for $\gamma = 4, 8, 16$, even though some deviating points enhanced the visual pattern.

Common for all correlations was that they all overlapped to a large degree at lower values for coherence bandwidth and ABF. There were thus many cases where a low coherence bandwidth did not require a high resolution. There was on the other hand less overlap in the right side regions for the different resolutions. It could therefore be concluded that there were thresholds for when it could be viewed as safe to use a certain resolution, while a lower resolution may have been of equal performance. If these values were used as thresholds for the frequency selection

algorithm, the BER could be decreased minimally while reducing the number of weight calculations performed. The overlaps would lead to higher resolutions than necessary being selected, but still lower the computational resources required which was the aim of the algorithm.

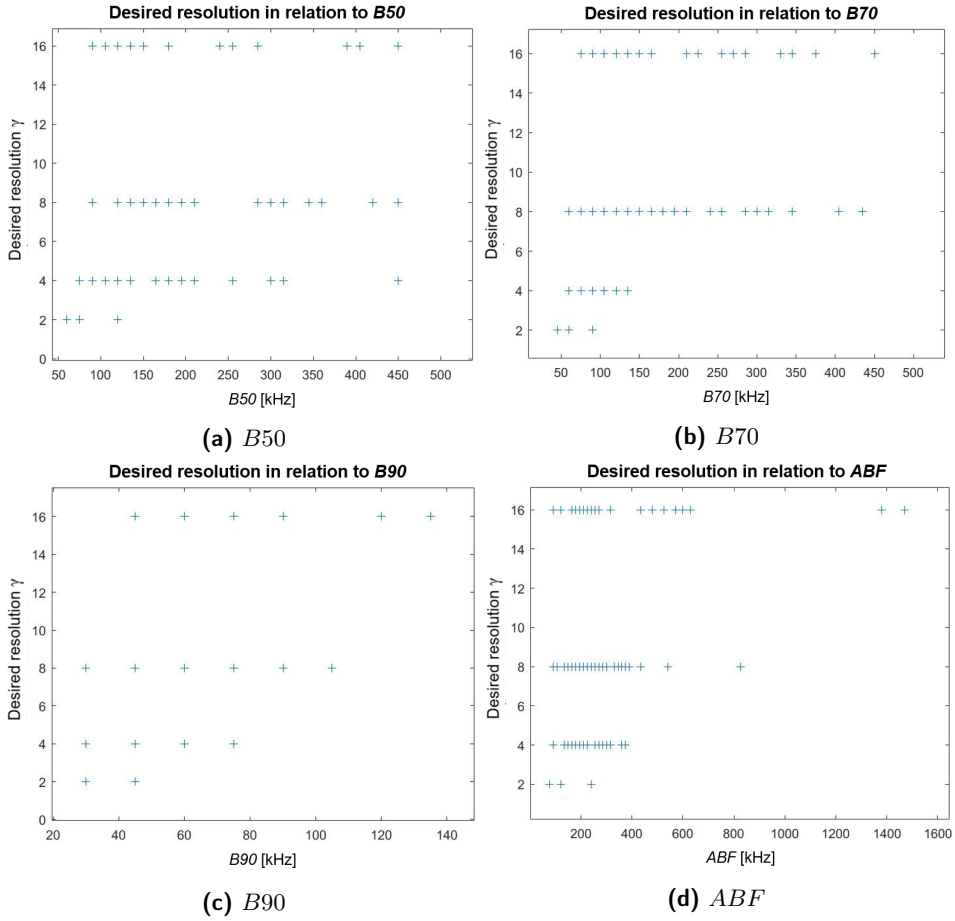

(a) $B50$ **(b)** $B70$

(c) $B90$ **(d)** ABF

Figure 8.1: Correlation between suitable resolution and ABF, $B90$, $B70$ and $B50$.

Instead of visually determining the thresholds from the plots, they were estimated by the statistics of the data points. To account for discrepancies, the thresholds were set to the first value below the 90th percentile for each resolution. Figure 8.2 shows the resolution regions for the four different measures. The range of Δf for which the correlation was calculated was set to 450 kHz. This limit was set with the motivation that very few channels reached the correlation level $B50$ at a larger frequency spacing. In the figure, one can observe that the three coherence bandwidth regions differed significantly. The $\gamma = 8, 16$ regions for $B50$

were completely missing, and the $\gamma = 4, 16$ regions for $B70$ were very small. Even with a larger span than 450 kHz, the regions for $B50$ were not clear. The $\gamma = 4, 8$ regions for $B90$ were small, but slightly larger than the previously mentioned ones. This corresponds well to the more clearly visible correlation pattern in Figure 8.1c. The $\gamma = 8, 16$ regions for ABF were also small due to the overlapping, but about as clear as for $B90$.

As the regions for $B90$ were most evenly spaced and consistent, it was chosen as the decision parameter for the algorithm when using coherence bandwidth as the decision parameter. The thresholds obtained from Figure 8.2 are also represented in Table 8.1, and were used in following simulations. The thresholds were computed on a PRB level, and would have to be adapted when using other numerologies.

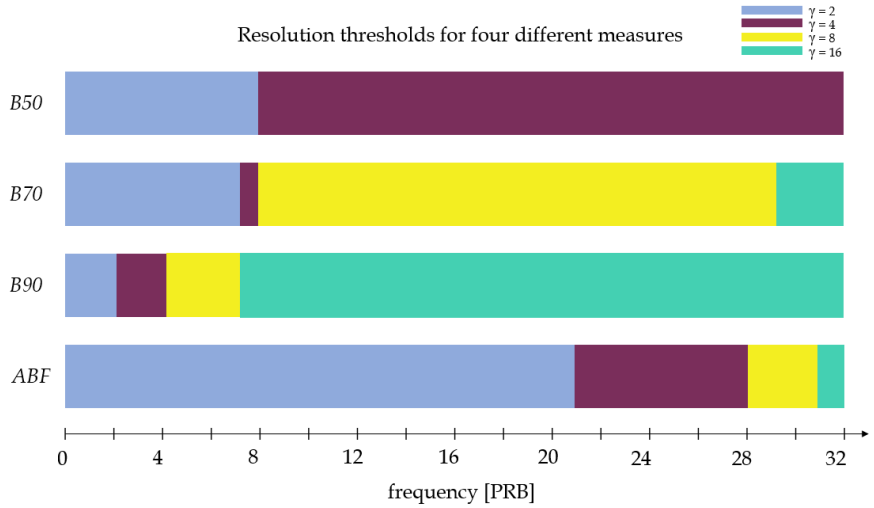

Figure 8.2: Resolution regions to be used for resolution selection algortihm. The measures are of the unit PRB in the frequency domain as the channel matrix is downsampled to PRB level before analyzing the frequency response.

Resolution γ [PRB]	ABF [PRB]	$B90$ [PRB]
2	0	0
4	21	2
8	28	4
16	31	7

Table 8.1: The thresholds for when a certain resolution should be chosen.

The thresholds for T_{rms} were found in the same way as for the other measures, see Figure 8.3, and are shown in Figure 8.4 and Table 8.2. The thresholds for T_{rms} were not calculated on a PRB level but on a time scale, which is why they are presented separately from ABF and coherence bandwidth.

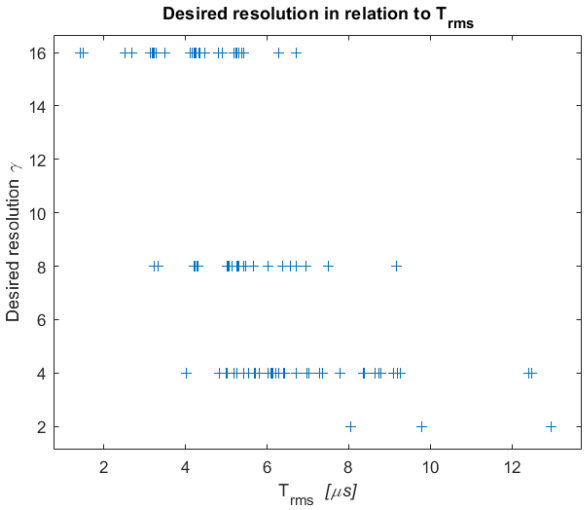

Figure 8.3: Correlation between suitable resolution and T_{rms}

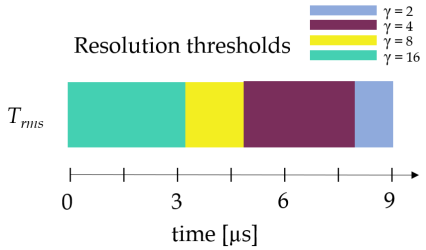

Figure 8.4: Resolution regions for T_{rms} to be used for resolution selection algortihm.

Resolution γ [PRB]	T_{rms} [μ s]
2	8.07
4	4.88
8	3.26
16	0

Table 8.2: The thresholds for when a certain resolution should be chosen.

The three measures are closely related to each other while having a few different properties. The main drawback of ABF is its noise sensitivity, which makes it a weak candidate in a real world application scenario. The coherence bandwdith, obtained from the frequency correlation function, is a less noise sensitive measure. The drawback is that it is not obvious how to take phase noise into account, which becomes especially impactful in a LOS scenario where the phase distribution will be heavily weighted. In this project, the coherence bandwidth was calculated from the absolute value of the FCF. This means that the phase differences are ignored, which could reduce the performance. The T_{rms} is the time domain represenation of the coherence bandwidth, where this issue is avoided as there is no phase to be accounted for. This makes T_{rms} a good candidate for the algorithm, alongside with the coherence bandwidth.

All thresholds estimated are valid in the simulation scenario specified, however it is likely that other thresholds would be needed for other scenarios. Different precoding techniques and channel models could be two factors that would affect these thresholds. The Winner II channel model is a simplified channel model and it is possible that the results would be closer to reality if an up-to-date 3GPP channel model was used.

8.2 Adaptive Resolution Simulation

The adaptive resolution simulations showed that the algorithm was able to select a suitable frequency resolution and maintain a BER comparable to that of a 2 PRB resolution. The following figures show the BER for three different channels, first for all resolutions and then for the resolutions chosen by the algorithm using coherence bandwidth as decision parameter. Lastly the total measured runtime for the weight calculations are displayed to show the lowered complexity.

Figure 8.5a shows a channel where the curves $\gamma = 2, 4$ are closely aligned, which implies that 4 PRB was a good resolutions choice. Figure 8.5b shows the selected resolutions for each SNR, and it can be seen that the algorithm correctly chose $\gamma = 4$ as the resolution for most SNR levels. It did choose $\gamma = 2$ for the first section, which shows that the algorithm was impacted by noise. Lower SNR ranges

where the BER is above 10^{-1} are however not as interesting when it comes to a real world scenario, as a much lower BER is desired for reliable communication.

Figure 8.6a shows a channel where the BER for $\gamma = 4, 8$ are closely aligned with the BER curve for $\gamma = 2$. This implicates that $\gamma = 8$ is a good resolution choice, which was also the resolution selected by the algorithm as can be seen in Figure 8.6b. For the channel in Figure 8.7, all the resolutions are closely aligned. The optimal resolution would then be $\gamma = 16$, which was also chosen by the algorithm with the exception of the lowest SNR level. The noise then caused the algorithm to choose a higher resolution. The two later figures show channels where the BER decreased fast, which is the reason there are no samples for higher SNR. The BER was then 0 for the amount of bits used.

The runtime decreased in all three scenarios for the lowered resolutions, see Figure 8.5c, Figure 8.6c and Figure 8.7c. In theory, there should be a linear correlation between the runtime and resolution. Half as many weight calculations would result in half the time spent computing them. The graphs instead show significant but smaller decrease in runtime. The downward trend at the end of each simulation seemed to be related to Matlab specific performance changes towards the end of the simulation. As these results were consistent over all simulations and all different SNR ranges tested, one possible reason for this could be that Matlab compiles the code while running. This might not be needed towards the end of the simulation, leaving more resources available for the weight calculations.

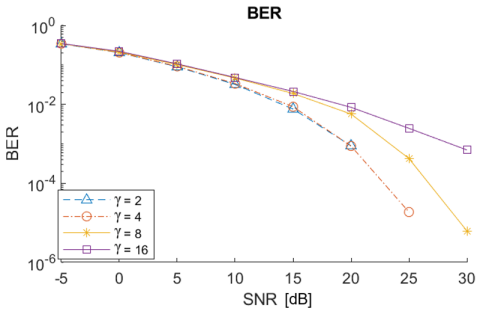

(a) BER for all resolutions

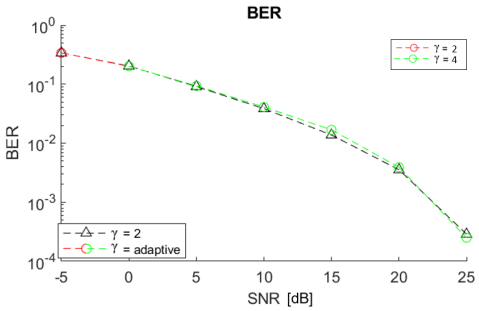

(b) BER for $\gamma = 2$ and adaptive resolution

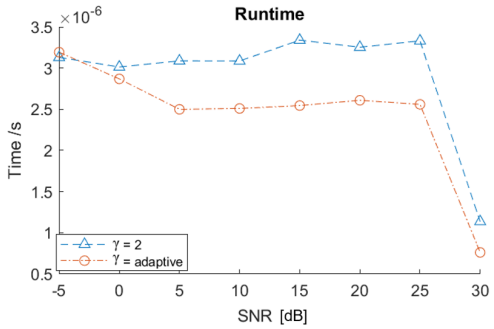

(c) Runtime for $\gamma = 2$ and adaptive resolution

Figure 8.5: BER for all resolutions and BER when selecting the resolution adaptively with the frequency resolution selection algorithm for the same channel. Including measured runtime difference.

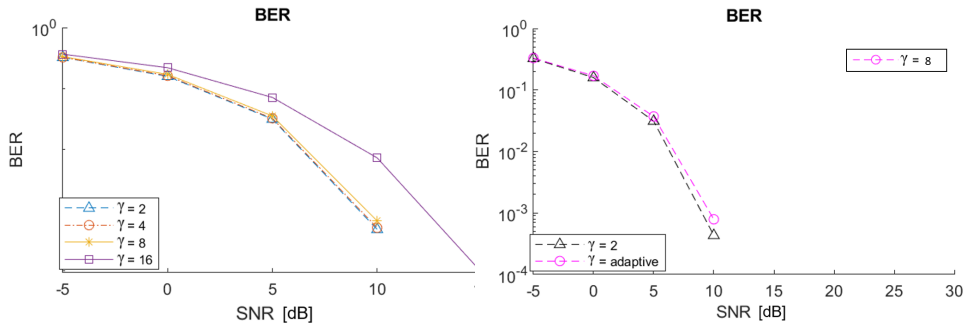

(a) BER for all resolutions **(b)** BER for $\gamma = 2$ and adaptive resolution

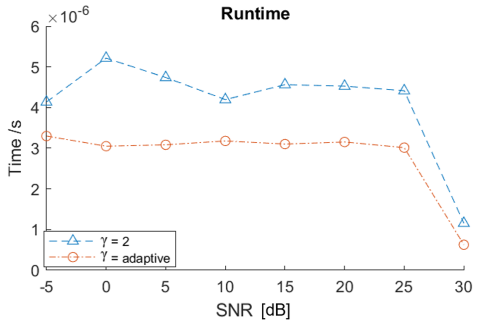

(c) Runtime for $\gamma = 2$ and adaptive resolution

Figure 8.6: BER for all resolutions and BER when selecting the resolution adaptively with the frequency resolution selection algorithm for the same channel. Including measured runtime difference.

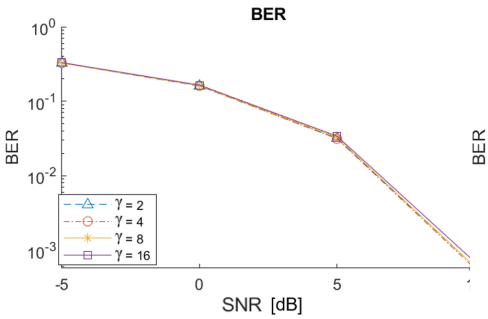

(a) BER for all resolutions

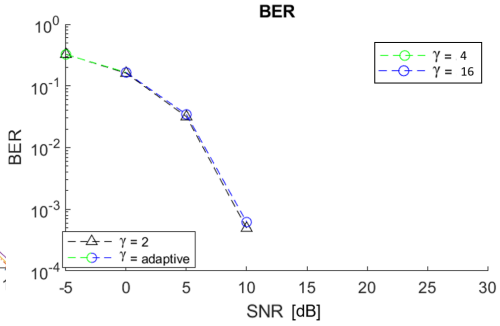

(b) BER for $\gamma = 2$ and adaptive resolution

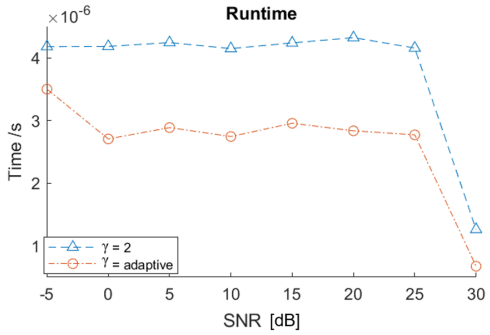

(c) Runtime for $\gamma = 2$ and adaptive resolution

Figure 8.7: BER for all resolutions and BER when selecting the resolution adaptively with the frequency resolution selection algorithm for the same channel. Including measured runtime difference.

To test the robustness of the algorithm, it was not enough to run the simulation for only a few channels. Table 8.3 shows the average increase of BER per SNR when running it for 100 different channels and using ABF, T_{rms} and coherence bandwidth ($B90$) as decision parameter. When using $B90$, the average increase of BER caused by the higher resolutions was 26.14%, and the average resolution chosen by the algorithm was 3.17 PRB. A resolution of $\gamma = 3.17$ means that the total resources required for the beamforming weight calculations decreased by 37% compared to using $\gamma = 2$. The average measured decrease in weight calculation runtime was 18%, which is less than the theoretical value of 37%. When using ABF, the average chosen resolution was instead 3.36 while the BER increased 8 times on average. Two of the channels gave a BER increase of more than a factor 100, meaning that the prediction was wrong but also that those two channels had an extreme impact on the average increase. Even though an increase of a factor 100 sounds extreme, it is not an uncommon difference for the BER between resolutions. It represents an increase from for example 10^{-4} to $10^{-}2$ in BER. With the two channels excluded, the average BER increase was instead 35.6 %. Even

then, the performance of the algorithm with ABF is barely comparable to that of $B90$. The thresholds were estimated using the highest SNR level for each channel. Due to its' extreme noise sensitivity, it is possible that the algorithm would show better performance if one threshold was estimated for each SNR level. This was not explored as it seems unlikely that the ABF measure would be found reliable enough to be used in product development.

The simulations for T_{rms} showed a BER increase of 8.2% with an average resolution of 4.47 PRB. The differences in BER increase between the three versions of the algorithm are small, while the chosen resolutions differ more. Using T_{rms} as decision parameter for the algorithm provides a very low increase of BER while choosing the highest average resolution. As discussed previously, the coherence bandwidth is based solely on the absolute value of the frequency correlation function, completely ignoring the phase differences. This issue is not present in the T_{rms} measure, which might be the reason for its' higher reliability and better performance.

SNR [dB]	0	5	10	15	20	25
BER increase $B90$ [%]	0.4	0.5	1.8	5.3	56.3	92.5
BER increase T_{rms} [%]	1.43	2	3.5	5.84	10.2	26.22
BER increase ABF [%]	0.2	2.6	5.2	30.6	257	4406

Table 8.3: Increase of BER per SNR when using the adaptive resolution algorithm

The results have thereby shown that this is an algorithm that lowers the complexity of the beamforming by reducing the resolution of the weight calculations. It has also been found that the rms delay spread, T_{rms}, is the measure best suited for a decision basis with an average resolution of 4.47 PRB and BER increase of 8.2%.

8.3 Number of Antennas Dependence

The thresholds found suitable for the resolution selection are shown in table 8.4. There is no clear correlation between the threshold values and the number of antennas. The size of the differences indicate that they are a result of different channels being generated for each of the antenna configurations. Generating the same channel with different number of antennas was not possible using the seed for the Winner II channel model, as the different number of antennas generate different channels with the same seed. Only basing the thresholds on the results of 200 channels will result in variances in the results, and it is thus possible that there could be small differences that would be visible with more extensive simulations.

Table 8.5 shows the average BER increase for the different number of antennas using their respective estimated thresholds. The results show that the performance of the algorithm is not affected by the number of antennas. It is possible that there are once again differences that are not measurable due to the small number of channels tested. The performance when varying the number of antennas is harder to evaluate through simulations than the different decision parameters. The reason for this is that the same channels could be generated for all different parameters, which made the results more comparable. In these simulations, 100 new channels were generated for each antenna configuration, causing the results to have more dependencies than only the number of antennas. For some channels, a faulty estimation can cause several hundreds of percent in BER increase, depending on the SNR level. If one antenna configuration happened to get only a few more of such a channel than the others, it would appear the performance was bad even though it was actually random. After further analyzing the reason for the higher percentage of BER increase in the 16 Tx case, it was clear that it was caused by these randomly generated channels where the estimation errors yielded very high BER increases.

The reliability of the results would be much higher if the simulations were run for a larger amount of channels. Despite this deficit, the results show that the algorithm works well regardless of the antenna array size.

	Thresholds [μs]		
Number of Antennas	4 PRB	8 PRB	16 PRB
8 Tx	0.114	0.065	0.054
16 Tx	0.115	0.06	0.051
32 Tx	0.116	0.071	0.063
64 Tx	0.124	0.075	0.05

Table 8.4: The lower limit for each resolution and each antenna configuration. The lower limit for 2 PRB is 0.

Number of Antennas	Mean BER Increase [%]	Average Resolution [PRB]
8 Tx	12.6	4.93 PRB
16 Tx	15.26	5.18 PRB
32 Tx	13.37	4.28 PRB
64 Tx	8.2	4.47 PRB

Table 8.5: Increase of BER per SNR using adaptive resolution based on T_{rms} for four different antenna configurations.

8.4 MU-MIMO Simulation with Two Users

The results show that the MU-MIMO case is significantly more affected by the change of resolution. A resolution of 1 RE gives a BER curve similar to the SU-MIMO cases, while the performance is significantly worse at resolutions as low as $\gamma = 1$. An example plot from one such simulation is shown in Figure 8.8. Lower resolutions than 1 RE seem to reach plateaus for when the BER does not decrease further, which is an effect of the interference between the signals to the different users not being cancelled out. As mentioned in secion 7.3.5, the MU-MIMO case therefore puts even more pressure on precise knowledge of the channel, and not even 1 PRB resolution is be good enough.

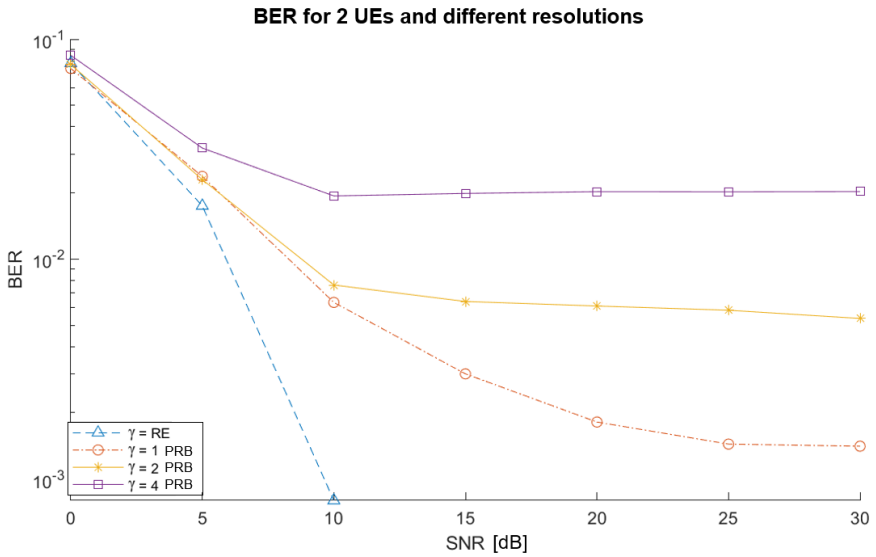

Figure 8.8: BER for different resolutions and 2 UEs in a MU-MIMO scenario.

8.5 BER Limit Algorithm Simulation

The simulations show that it is possible to set a threshold and adapt the resolution to the lowest one that satisfies the BER limit criterion. Figure 8.9 shows two examples of different channels where the algorithm has been used with a BER limit of 10^{-1}, where the first channel suffers a significant increase of BER and the second one does not. As indicated in previous simulations, this depends on the frequency selectivity of the channel. The average BER for 100 channels is shown in Figure 8.10, displaying a clear increase of BER compared to that of the 2 PRB resolution curve, while keeping under the BER limit of 10^{-1} where possible. Table

8.6 presents these values in numbers. The average chosen resolution was 13.5 PRB, reducing the number of weight calculations by 85%.

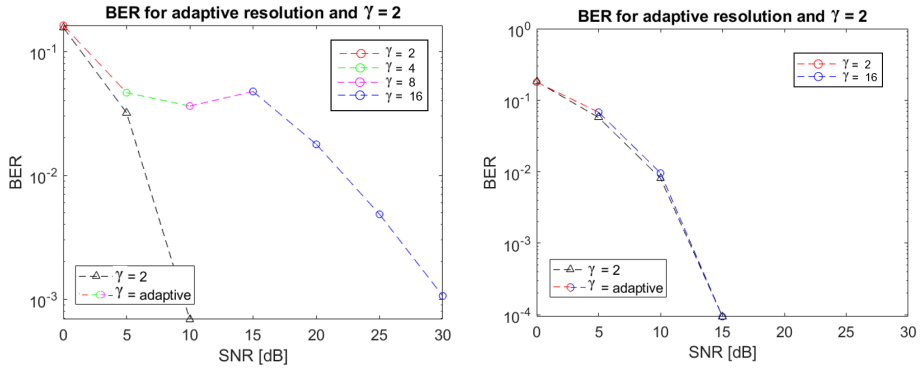

(a) Channel 1 **(b)** Channel 2

Figure 8.9: BER for resolution 2 PRB and adaptive resolution.

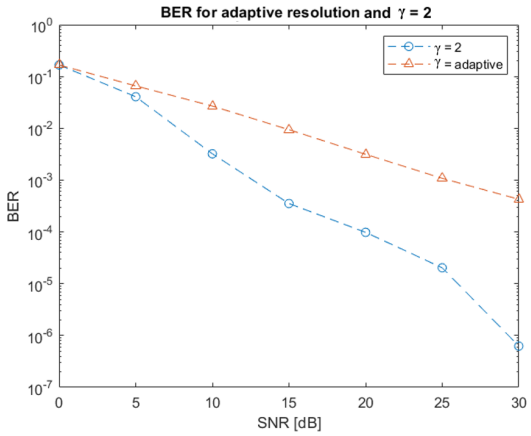

Figure 8.10: Average BER for resolution 2 PRB and adaptive resolution using the BER limit algorithm with a 10^{-1} BER limit.

SNR [dB]	0	5	10	15	20	25	30
BER $\gamma = 2$	0.167	0.041	0.0032	0.0004	0.0001	0	0
BER $\gamma =$ adaptive	0.167	0.066	0.027	0.0094	0.0032	0.0011	0.0004

Table 8.6: BER for the 10^{-1} BER limit algorithm

When setting the BER threshold to 10^{-2}, the results were very similar. Fig-

ure 8.11 shows the algorithm performance for two different channels, again with varying results. The difference is that the resolution is not lowered until the SNR where the BER is below 10^{-2}. This can also be observed in Figure 8.12, where the curve for the adaptive resolution follows that of the 2 PRB resolution until the threshold is reached. The values for the curves are presented in Table 8.7. The average chosen resolution was 12.3 PRB, reducing the number of weight calculations by 84%.

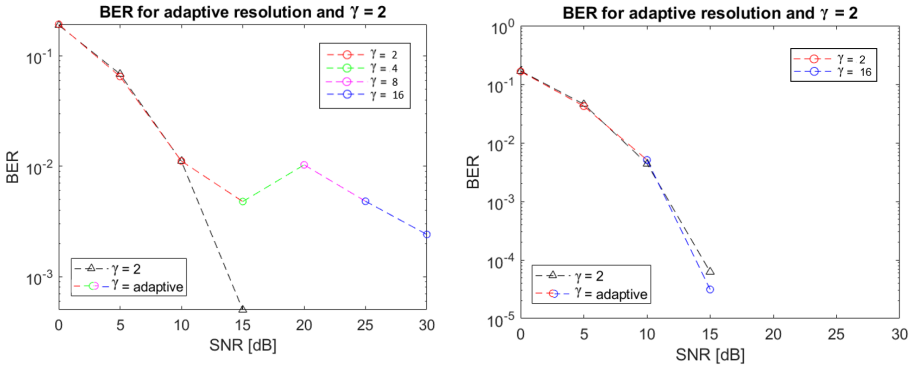

(a) Channel 1 **(b)** Channel 2

Figure 8.11: BER for resolution 2 PRB and adaptive resolution.

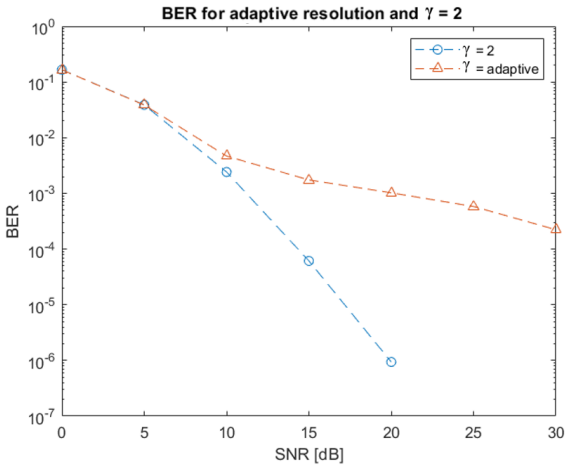

Figure 8.12: Average BER for resolution 2 PRB and adaptive resolution using the BER limit algorithm with a 10^{-2} BER limit.

SNR [dB]	0	5	10	15	20	25	30
BER $\gamma = 2$	0.166	0.039	0.0024	0.0001	0	0	0
BER $\gamma =$ adaptive	0.165	0.039	0.0047	0.0017	0.001	0.0006	0.0002

Table 8.7: BER for the 10^{-2} BER limit algorithm

Chapter 9

Conclusions and Future Work

In the thesis we have investigated the possibility to adapt the frequency resolution of the beamforming weight calculations. It is clearly possible to predict for what channel conditions the resolution can be lowered without significant performance loss. The results show that the required resolution is dependent on the frequency selectivity of the channel, and that analysis of it can serve as a foundation for the resolution selection. Incorporation of the algorithm in a product would reduce complexity and leave computational power free for other functionality.

The thresholds would then likely have to be evaluated further as the simplified simulation does not entirely represent a real world scenario. The Winner II channel model is the main reason for this deviance, as it is much less complex than a real world scenario. As previously mentioned, the resemblance with reality could be enhanced by a more advanced channel model. With this in mind, the Winner II model was still determined to be sufficient to exemplify an initial version of the algorithm.

The two algorithms presented in the thesis both have potential to be used in application. It is clear that the first algorithm, optimizing the resolution while maintaining the same BER, has great potential in any product that performs digital beamforming. The lowered complexity results in little to no decrease in performance, which is always desireable. The other algorithm, minimizing the resolution while keeping the BER under a threshold, results in a substantial performance loss. It does, however, allow more than twice as high resolution than the first version of the algorithm, which might make it useful in scenarios where the computational resources are very scarce. It can therefore be argued that both algorithms have great potential in opening further possibilities for any product using beamforming, as the complexity might not have to become a limitation. Seeing that the concepts of MIMO and beamforming are considered necessities for NR and future generations cellular systems, functionality like this could become key.

One future scope on the topic could be to use machine learning for the frequency

response analysis. Even though the correlation is strong enough to yield good results, it is possible that there are certain properties in the channel estimation that affect the impact of the resolution while not being prominent in coherence bandwidth, ABF or delay spread measures. It would be interesting to see if the algorithm could become even more robust with this addition, and explore if there are such hidden properties in the channel.

Running the simulation for only 200 channels to predict the thresholds and then using the 90th percentile as a reference might result in larger variations than desired. To reduce these uncertainties, the simulation would have to be run for a larger number of channels. In this thesis, there was not enough time for this, and the presented method was determined to be sufficient for the thesis. It would of course also be of interest to test the impact of the resolution in a lab environment. That would give a better idea of the potential of the technology in a real world scenario.

If the algorithms were to be implemented in a product, it could be beneficial to extend them to also take the hardware load of the base station and QoS requirements of the user into account. This would provide a more extensive resolution selection where the algorithms could trade hardware resources for QoS improvements to meet the user requirement. Overall, there are many applications and extensions of the adaptive resolution technology that have great potential in both today's and future generations of cellular communications.

References

[1] 3GPP. *5G NR Physical Layer Procedures for Control*. ETSI, 2018.

[2] 3GPP. *5G NR Physical Channels and Modulation*. ETSI, 2018

[3] 3GPP. *5G NR Physical Layer Procedures for Data*. ETSI, 2018.

[4] T. Bi, X. Chen. *Research on the Linear Precoding Algorithm Based on 5G Mobile Communication Technology* IEEE International Conference on Artificial Intelligence and Information Systems (ICAIIS), 2020.

[5] R. J. C. Bultitude. *Estimating Frequency Correlation Functions From Propagation Measurements on Fading Radio Channels: A Critical Review* IEEE Transactions on Selected Areas in Communications, VOL. 20, NO. 6, Aug. 2002.

[6] E. Dahlman, S. Parkvall, J. Peisa, H. Tullberg. *5G Evolution and Beyond*. 2019 IEEE 20th International Workshop on Signal Processing Advances in Wireless Communications (SPAWC), 2019.

[7] E. Dahlman, S. Parkvall, J. Sköld. *5G NR The Next Generation Wireless Access Technology*. Elsevier, 2018.

[8] R. Doostnejad. *Precoding and Beamforming for Multi-Input Multi-Output Downlink Channels* Ph.D. dissertation, The Edward S. Rogers Sr. Department of Electrical and Computer Engineering University of Toronto, 2005.

[9] N. Fatema, G. Hua, Y. Xiang, D. Peng. *Massive MIMO Linear Precoding: A Survey* IEEE Systems Journal, VOL. 12, NO. 4, December 2018.

[10] X. Gao, O. Edfors, F. Rusek, F. Tufvesson. *Linear pre-coding performance in measured very-large MIMO channels* Proc. of the 74th IEEE Vehicular Technology Conference, 2011

[11] J. Guirado López.Puigcerver *Design and optimization of Bandwidth Part selection for massive beamforming* Master Thesis at Lund University, Department of Electrical and Information Technology, 2020

[12] S. Guo, X. Hou, H. Wang. *Dynamic TDD and Interference Management towards 5G* IEEE Wireless Communications and Networking Conference (WCNC), 2018.

[13] P. Kyösti, J. Meinilä, L. Hentilä *WINNER II Channel Models* IST-4-027756 WINNER II D1.1.2 V1.2, 2007

[14] M. Lentmaier. *EITN70 Channel Coding for Reliable Communication* Course Book, Lund University, Department of Electrical and Information Technology. Lund, October 2018.

[15] S. Mathur. *Small Scale Fading in Radio Propagation* 16:332:546 Wireless Communication Technologies Spring, 2005.

[16] A F. Molisch. *Wireless Communications, Second Edition* John Wiley & Sons, 2011 p27, p82, p385, p256-p257, p445-p488

[17] M. Nadder Hamdy *Beamformers Explained* CommScope, 2020

[18] L. D. Nguyen, H. D. Tuan, T. Q. Duong, and H. V. Poor. *Multi-user regularized zero-forcing beamforming* IEEE Transactions on Signal Processing, 2019.

[19] S. Noh, M D. Zoltowski. *Multi-Resolution Codebook and Adaptive Beamforming Sequence Design for Millimeter Wave Beam Alignment.* IEEE Transactions on Wireless Communications, 2017.

[20] S. Onoe. *Evolution of 5G Mobile Technology Toward 2020 and Beyond.* ISSCC, 2016.

[21] J. Peisa, P. Persson, E. Dahlman, S.Parkvall. *5G Evolution, 3GPP Release 16 & 17 overview* Ericsson Technology Review, February 2020.

[22] M. Sánches Varela, M. García Sánches *RMS Delay and Coherence Bandwidth Measurements in Indoor Radio Channels in the UHF Band* IEEE Transactions on Vehicular Technology, VOL. 50, NO. 2, March 2001.

[23] N. Sathish Kumar, K. R. Shankar Kumar *Performance analysis and comparison of m x n zero forcing and MMSE equalizer based receiver for mimo wireless channel* Songklanakarin J. Sci. Technol. May - June 2011

[24] K. Titus, Y. Lo *Maximum Ratio Transmission* IEEE Transactions of Communications, VOL. 47, NO. 10, October 1999.

[25] K. Witrisal, A. Bohdanowicz. *Influence of Noise on a Novel RMS Estimation Method Delay Spread* 11th IEEE International Symposium on Personal Indoor and Mobile Radio Communications, 2000.

[26] K. Witrisal, K. Yong-Ho, R. Prasad. *A New Method to Measure Parameters of Frequency-Selective Radio Channels Using Power Measurements* IEEE Transactions on Communications, VOL. 49, NO. 10, October 2001.

[27] D. Wout, F. Arne, C. Iñigo. *RMS Delay Spread vs. Coherence Bandwidth from 5G Indoor Radio Channel Measurements at 3.5 GHz Band* Sensors (Basel). 20(3): 750. February 2020.

Printed by Tryckeriet i E-huset, Lund 2021

LUND
UNIVERSITY

Series of Master's theses
Department of Electrical and Information Technology
LU/LTH-EIT 2021-834
http://www.eit.lth.se